Journal Pre-proof

Periodic response of a nonlinear axially moving beam with a nonlinear energy sink and piezoelectric attachment

Danilo Karličić, Milan Cajić, Stepa Paunović, Sondipon Adhikari

PII: S0020-7403(20)34335-6
DOI: https://doi.org/10.1016/j.ijmecsci.2020.106230
Reference: MS 106230

To appear in: *International Journal of Mechanical Sciences*

Received date: 18 November 2019
Revised date: 9 December 2020
Accepted date: 10 December 2020

Please cite this article as: Danilo Karličić, Milan Cajić, Stepa Paunović, Sondipon Adhikari, Periodic response of a nonlinear axially moving beam with a nonlinear energy sink and piezoelectric attachment, *International Journal of Mechanical Sciences* (2020), doi: https://doi.org/10.1016/j.ijmecsci.2020.106230

This is a PDF file of an article that has undergone enhancements after acceptance, such as the addition of a cover page and metadata, and formatting for readability, but it is not yet the definitive version of record. This version will undergo additional copyediting, typesetting and review before it is published in its final form, but we are providing this version to give early visibility of the article. Please note that, during the production process, errors may be discovered which could affect the content, and all legal disclaimers that apply to the journal pertain.

© 2020 Published by Elsevier Ltd.

Journal Pre-proof

Highlights

- Approximate procedure to design nonlinear energy sink with a piezoelectric energy harvesting device for reducing amplitudes of the axially moving beams.
- Grounded configuration of nonlinear energy sink piezoelectric energy harvesters model is adopted.
- Frequency-amplitude responses curves are determined by incremental harmonic balance and continuation methods.
- The short time energy transfer and localization to the nonlinear energy sink from the axially moving beam.

Journal Pre-proof

Graphical abstract

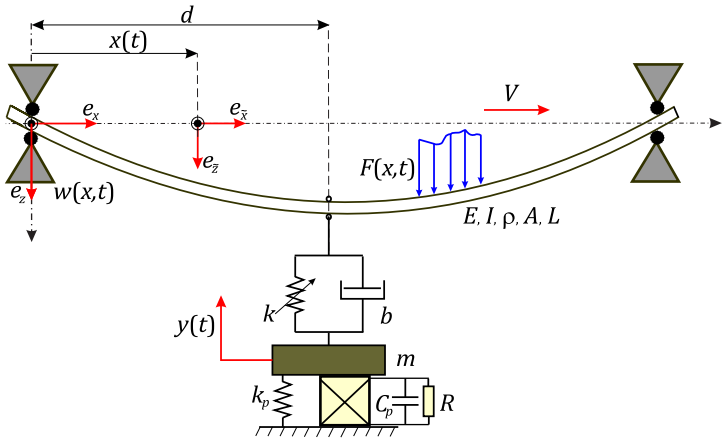

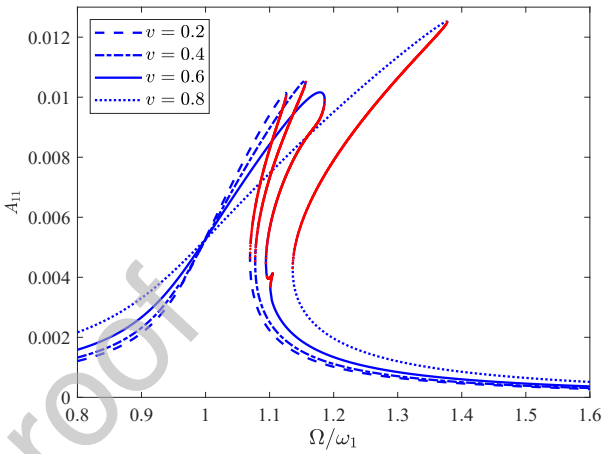

Journal Pre-proof

Journal Pre-proof

Periodic response of a nonlinear axially moving beam with a nonlinear energy sink and piezoelectric attachment

Danilo Karličić [a,b,*], Milan Cajić [b], Stepa Paunović [b], Sondipon Adhikari [a]

[a] *College of Engineering, Swansea University, United Kingdom*
[b] *Mathematical Institute of the Serbian Academy of Sciences and Arts, Kneza Mihaila 36, Belgrade, Serbia*

Abstract

An efficient semi-numerical framework is used in this paper to analyze the dynamic model of an axially moving beam with a nonlinear attachment composed of a nonlinear energy sink and a piezoelectric device. The governing equations of motion of the system are derived by using the Hamilton's principle with von Karman strain-displacement relation and Euler - Bernoulli beam theory. The nonlinear energy sink is modeled as a lumped - mass system composed of a point mass, a spring with nonlinear cubic stiffness and a linear viscous damping element. The piezoelectric device is placed in the ground configuration. Frequency response curves of the presented nonlinear system are determined by introducing the incremental harmonic balance and continuation method for different values of material parameters. Based on the Floquet theory, the stability of the periodic solution was determined. Moreover, the presented results are validated with the results obtained by a numerical method as well as the results from the literature. Numerical examples show a significant effect of the nonlinear attachment on frequency response diagrams and vibration amplitude reduction of the primary beam structure.

Keywords: Axially moving beam, Nonlinear energy sink, Vibration attenuation, Incremental harmonic balance, Frequency response.

1. Introduction

Vibration studies of axially moving and spinning beams have attracted considerable attention of the scientific community since such models are extensively used in different industrial fields and aerospace engineering. Some typical examples of the engineering applications include, but are not limited to, rotary drill-strings in oil wells, drilling machines in manufacturing, Cardan shafts of automobiles, extrusion processes, deployment of appendages in space, robotic manipulators, telescopic members of loading vehicles, machine tools and chain-saw blades [1–3]. However, undesired vibration and instabilities can cause failures of such structures over time and it is crucial to reduce vibration amplitudes by using passive, semi-active or active vibration absorbers or any combination there of [4].

In a wide spectrum of engineering applications, a nonlinear energy sink (NES) is introduced as a passive nonlinear vibration absorber. The main feature of the NES is to transfer the mechanical energy from a primary structure to the nonlinear attachment. This concept has several advantages such as simple configuration, high robustness and broadband vibration attenuation properties [4, 5]. It is well known that linear vibration absorbers attenuate vibrations of the main structure by redistribution of its vibration energy through spring and attached additional masses. However, NES composed of a nonlinear spring, weak damper and a point mass has wider frequency bandwidth of attenuation due to strong nonlinear stiffness. The first model of NES was introduced by Vakakis and his co-workers [6–8]. Afterwards, this concept evolved with the introduction of different nonlinear characteristics such as the nonlinear cubic stiffness [6], polynomial stiffness [9], non-smooth stiffness [10], different types of the nonlinear damping models [11], vibro-impact models [12], chatter control [13] and multiple degrees of freedom NES systems [14, 15]. Moreover, the combination of NES with an energy harvesting device allows conversion of mechanical energy to electrical energy as shown in [16]. The main physical phenomenon that occurs in NES is the targeted energy transfer (energy pumping), where a certain amount of mechanical energy given to the main structure is transiently transmitted to NES, as shown in some experiments [17, 18].

*Corresponding author
Email address: danilo.karlicic@swansea.ac.uk (Danilo Karličić)

Journal Pre-proof

One particular application of NES attachments is in structural dynamic models, where the primary structure is based on continuous elements such as strings [19], beams [20], pipes [21], plates [22] or wings [23]. Recently, the interest in such models has increased, especially in mechanical, civil engineering and aerospace applications for vibration suppression and control. For example, in some research work, special attention is paid to axially-moving structures with NES [24], where the authors mostly considered linear models for primary structures with nonlinear attachments. Moreover, the problems with nonlinear axially moving strings or beams with NES or NES-EH models are addressed in a limited number of studies. In this paper, our attention will be primarily focused on the application of a nonlinear model of an axially moving beam with NES-EH device. In the series of papers, Li-Qun Chen and co-workers analyzed different structural models with NES, starting from a new discrete NES with inertia [25, 26], axially moving beam with NES and considered thermal shock and impulse induced vibration [27, 28], and finally vibration reduction in a spacecraft [29]. They used both theoretical and experimental approaches in order to analyze the effects of NES on primary structures. Zhang et al. [30] successfully controlled vibration response of an axially moving string by introducing NES into the system, where a numerical approach was employed to obtain the frequency response of the system. On the other hand, Zulli and Luongo [31, 32] have shown the effect of the attached NES on the vibration of a nonlinear string model by using the perturbation multiple scales and harmonic balance methods based on transient analyses for both the internal resonant and non-resonant cases.

In recent years, there has been an increased effort to develop efficient energy harvesting devices [33]. Different NES configurations coupled with energy harvesting devices were addressed in the literature to achieve both efficient vibration suppression and energy harvesting. Kremer and Liu [34] investigated energy harvesting using a nonlinear energy sink of a specific configuration with essential non-linearity and low damping. They studied the transient behavior of the system and demonstrated that the proposed apparatus is capable of harvesting energy in a broadband manner. In another study, the same group of authors [35] focused on harmonically forced responses of the system and investigated the steady-state responses analytically and experimentally. The results have shown typical behavior for NES and broadband energy harvesting and vibration attenuation capabilities. Zhang et al. [36] developed an energy harvester utilizing the localized vibration energy from NES, where the electrical energy is obtained by using the direct piezoelectric effect. Through the experimental and numerical analysis, the authors confirmed that NES based piezoelectric energy harvester is effective in vibration suppression of the primary system with significant broadband voltage output. Another approach in the analysis of the dynamics of a nonlinear energy sink with an integrated piezoelectric energy harvester was applied in a paper by Li et al. [37], where the complexification-averaging method was employed to examine vibration absorption and study the dynamic behavior of the observed system. Another concept of energy harvesters coupled with NES was used by Blanchard et al. [38], where vortex-induced vibration (VIV) of a cylinder is suppressed with an internal dissipation due to rotational NES. They designed NES suggesting its application in energy harvesting from VIV in submarine flows in order to generate electric power. Recently, Rasil Raj and Santhosh [39] studied the two-degree-of-freedom nonlinear system acting simultaneously as a vibration absorber and an energy harvester. The authors used the multi-harmonic balance method together with the arc-length continuation to generate frequency response curves for different values of system parameters. They additionally contributed to this subject by performing the optimization procedure based on genetic algorithm in combination with response surface methodology to generate the optimal frequency response of a multi-functional energy harvesting system.

The main purpose of this paper is to analyze a novel model of axially moving nonlinear beam with an attached NES-EH device for vibration reduction purposes. Moreover, by introducing the nonlinear attachment in the ground configuration the classical NES can be extended with EH capeability thus producing a unified device for vibration control as shown in [7, 40]. In order to study the proposed nonlinear system, we will introduce the methodology based on the IHB, Floquet stability theory and continuation methods for obtaining the amplitude-frequency responses in the the primary resonance state. The mathematical model of the axially moving beam is derived by using the Hamilton principle and the Euler-Bernoulli beam theory, and it is afterwards discretized by the Galerkin method. The effect of the NES-EH attachment on the axially moving beam is presented in frequency response diagrams and verified with the results from the literature. In general, the proposed methodology is suitable for determination of the amplitude-frequency curves of a strongly nonlinear system. The accuracy of the IHB method was demonstrated by comparing the results with those obtained through direct numerical integration and fine agreement is achieved. From the physical viewpoint, the axially moving beam with the nonlinear attachment composed of coupled NES and EH devices, can be used as a tensioner in the belt drive system [41], which is an excellent example of the application

Journal Pre-proof

of coupled NES-EH devices for simultaneous vibration reduction and energy harvesting purposes.

2. Problem formulation

2.1. Mechanical model

Let us consider a slender axially moving beam influenced by a transverse periodic force $F(x,t)$, with a NES and a piezoelectric device attached at distance d from the origin, as shown in Fig. 1. It is assumed that the transport velocity is constant V and the attachment is modeled as a lumped - mass system. The mechanical model of the nonlinear energy sink is composed of one nonlinear spring (of stiffness k) and one linear dashpot element (of damping b) connected to the point mass m. Moreover, the piezoelectric device is placed in ground configuration, where stiffness, loaded resistance and capacitance are given as k_p, R, C_p, respectively. The piezoelectric device is introduced for the EH purpose. The adopted model of the axially moving beam is based on the Euler - Bernoulli beam theory with the following properties: YoungâĂŹs modulus E, mass density ρ, length L, cross-section area A, the moment of inertia I, and simply supported boundary conditions. The x-coordinate is taken along the length of the axially moving beam and the z-coordinate is in the thickness direction of a beam. It should also be noted that the bending vibration of an axially moving beam occurs in the thickness direction with transverse displacement denoted by $w(x,t)$ and axial displacement by $u(x,t)$.

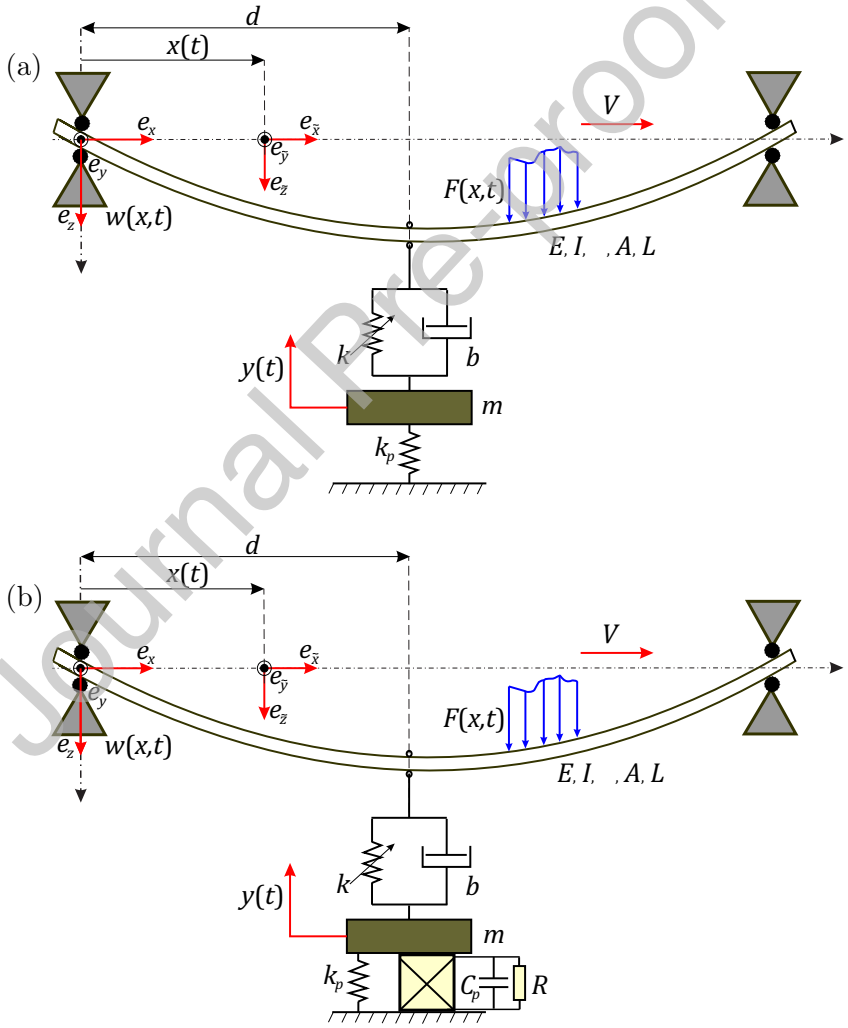

Figure 1: Mechanical model of an axially moving beam with a nonlinear attachment, a) Nonlinear energy sink (NES), and b) Nonlinear energy sink with an energy harvester NES-EH.

2.2. The equations of motion

In order to derive a differential equation of motion of the axially moving beam, we will introduce a few assumptions. First, we neglect the cross-sectional rotary inertia and the shear deformation, in line with the

Journal Pre-proof

Euler - Bernoulli beam theory. Secondly, we assume that the beam is influenced by the constant tension force P during movement with constant transport speed V. We introduce two reference systems where the first one is inertial, based on the origin with unit vectors $\mathbf{e}_x, \mathbf{e}_z$ and the corresponding coordinates (x, z), with the frame $\mathbf{e}_{\bar{x}}, \mathbf{e}_{\bar{z}}$ moving in the x direction with speed V. In this case, the ***displacement*** and the ***velocity vector*** of an arbitrary point M of the axially moving beam are given as

$$\mathbf{p}_M(x,t) = [u(x,t) + x(t)]\,\mathbf{e}_x + w(x,t)\mathbf{e}_z, \tag{1}$$

$$\mathbf{v}_M(x,t) = \frac{d\mathbf{p}_M}{dt}(x,t) = [u_{,t} + u_{,x}\,V + V]\,\mathbf{e}_x + (w_{,t} + w_{,x}\,V)\mathbf{e}_z, \tag{2}$$

where $V = \dfrac{dx}{dt}$. The constitutive equation is given in the following form

$$\sigma_{xx}(x,t) = E\varepsilon_{xx}(x,t) = E\left[u_{,x} - zw_{,xx} + \frac{1}{2}(w_{,x})^2\right], \tag{3}$$

where $\sigma_{xx}(x,t)$ and $\varepsilon_{xx}(x,t)$ represents the normal stress and von Karman's strain, respectively. The differential equations of motion can be derived by introducing the Hamilton's principle in the following form

$$\delta \int_{t_1}^{t_2} [K - (U + W)]dt = 0, \tag{4}$$

where δ is the variation operator, K and U represent the kinetic and the potential energy, respectively, and W is the work of external forces, and these are given given as

$$K = \frac{\rho A}{2}\int_0^L (v_M)^2 dx, \tag{5}$$

$$U = \frac{1}{2}\int_V \sigma_{xx}\epsilon_{xx}dx,$$

$$W = \int_0^L \left[\frac{1}{2}P(w_{,x})^2 - F(x,t)w\right]dx.$$

Introducing the relations Eq.(5) into Eq.(4), and using the methodology presented in [42, 43], we get the following system of differential equations for the axial and transverse displacements

$$\rho A\left[\ddot{u} + 2V\dot{u}_{,x} + V^2 u_{,xx}\right] - EA\left[u_{,xx} + w_{,x}\,w_{,xx}\right] = 0, \tag{6}$$

$$\rho A\left[\ddot{w} + 2V\dot{w}_{,x} + V^2 w_{,xx}\right] + EIw_{,xxxx} - \left[\left(P + EAu_{,x} + \frac{1}{2}EA(w_{,x})^2\right)w_{,x}\right]_{,x} = F(x,t), \tag{7}$$

with the corresponding simply supported boundary conditions as shown in [43, 44]. In order to analyze the transverse vibration of axially moving beams with NES-EH Fig. 1, we will neglect the axial vibration mode $u(x,t)$ by assuming a weak coupling between axial and transverse vibration modes [44, 45] and extend Eq.(7) with additional terms through Dirac delta function and external concentrated load as shown in [16, 46],

$$\rho A\left[\ddot{w} + 2V\dot{w}_{,x} + V^2 w_{,xx}\right] + EIw_{,xxxx} - \left[\left(P + \frac{1}{2}EA(w_{,x})^2\right)w_{,x}\right]_{,x} \tag{8}$$

$$+ \left\{k\left[w(d,t) - y(t)\right]^3 + b\left[\dot{w}(d,t) - \dot{y}(t)\right]\right\}\delta(x-d) = F(x,t),$$

$$m\ddot{y} + k\left[y(t) - w(d,t)\right]^3 + b\left[\dot{y}(t) - \dot{w}(d,t)\right] + k_p y(t) - \frac{\theta}{C_p}Q(t) = 0, \tag{9}$$

$$R\dot{Q}(t) - \frac{\theta}{C_p}y(t) + \frac{1}{C_p}Q(t) = 0. \tag{10}$$

Differential equations given in Eq.(8) - Eq.(10) describe the presented system with NES-EH device (see Fig.(1)), where $y(t)$ represents displacement of a point mass m, $Q(t)$ is the output electrical charge and θ is the electro-mechanical coupling coefficient as defined in [46].

By introducing the dimensionless quantities:

$$t^* = t\sqrt{\frac{P}{\rho A L^2}}, \quad w^* = \frac{w}{L}, \quad x^* = \frac{x}{L}, \quad y^* = \frac{y}{L}, \quad v^* = V\sqrt{\frac{\rho A}{P}}, \tag{11}$$

$$d^* = \frac{d}{L}, \quad v_1 = \sqrt{\frac{EA}{P}}, \quad v_f = \sqrt{\frac{EI}{PL^2}}, \quad k^* = \frac{kL^3}{P}, \quad b^* = \frac{b}{\sqrt{P\rho A}},$$

$$Q^* = \frac{Q(t)}{\theta L}, \quad \tilde{R} = \frac{C_p R}{L}\sqrt{\frac{P}{\rho A}}, \quad \tilde{G} = \frac{\theta^2 L}{C_p P}, \quad \varepsilon = \frac{m}{\rho A L}, \quad \tilde{k}_p = \frac{k_p L}{P}, \quad F^* = \frac{FL}{P},$$

into Eq.(8)-Eq.(10) and omitting asterisk notation yields dimensionless equations of motion of the axially moving beam with NES-EH attachment in the following form

$$\left[\ddot{w} + 2v\dot{w}_{,x} + v^2 w_{,xx}\right] + v_f^2 w_{,xxxx} - \left[\left(1 + \frac{1}{2}v_1^2 (w_{,x})^2\right) w_{,x}\right]_{,x} \tag{12}$$

$$+ \left\{k\left[w(d,t) - y(t)\right]^3 + b\left[\dot{w}(d,t) - \dot{y}(t)\right]\right\}\delta(x-d) = F(x,t),$$

$$\varepsilon\ddot{y}(t) + k\left[y(t) - w(d,t)\right]^3 + b\left[\dot{y}(t) - \dot{w}(d,t)\right] + \tilde{k}_p y(t) - \tilde{G}Q(t) = 0, \tag{13}$$

$$\tilde{R}\dot{Q}(t) - y(t) + Q(t) = 0. \tag{14}$$

In this paper, the symbol $\dot{(\cdot)}$ represents $\partial(\cdot)/\partial t$, $(\cdot)_{,x}$ is $\partial(\cdot)/\partial x$, $(\cdot)_{,xx}$ denotes $\partial^2(\cdot)/\partial x^2$ and so on for derivatives of higher order.

3. Approximate method

3.1. The Galerkin discretization

In order to discretize the partial differential equation of the presented model of the axially moving beam with nonlinear attachment and reduce it to a system of ordinary differential equations, we will apply the Garlekin method [47]. The discretization process leads to a mathematical model with finite number of degrees of freedom where the nonlinear modal coupling is taken into account. Therefore, within the framework of this paper, the solution of the partial differential equation Eq.(8) will be approximated by expanding the transverse displacement $w(x,t)$ into the series of admissible functions $\phi_j(x)$ that satisfy the boundary conditions, and time functions $q_j(t)$. The approximated solutions for transverse displacement $w(x,t)$ and external load $F(x,t)$ are given as

$$w(x,t) = \sum_{j=1}^{N} q_j(t)\phi_j(x), \tag{15}$$

$$F(x,t) = \sum_{j=1}^{N} f_j(t)\phi_j(x), \tag{16}$$

where $\phi_j(x) = \sin(j\pi x)$ satisfies the simply supported boundary conditions, and the time periodic function is given as $f_j(t) = f_j \sin\omega t$. The terms f_j and ω represent amplitude and frequency of the external load, respectively.

Inserting Eq.(15) and Eq.(16) into Eq.(12), and taking into account the orthogonality conditions, we will obtain a system of N ordinary differential equations as follows

$$\sum_{j=1}^{N} M_{ij}\ddot{q}_j + \sum_{j=1}^{N} C_{ij}\dot{q}_j + \sum_{j=1}^{N} K_{ij}q_j + \sum_{j=1}^{N}\sum_{r=1}^{N}\sum_{g=1}^{N} \tilde{K}_{ijrg}q_j q_r q_g + \tag{17}$$

$$\left\{k\left[\sum_{j=1}^{N} q_j\phi_j(d) - y\right]^3 + b\left[\sum_{j=1}^{N}\dot{q}_j\phi_j(d) - \dot{y}\right]\right\}\phi_i(d) = \tilde{f}_{ij}\cos(\Omega t),$$

where

$$M_{ij} = \int_0^1 \phi_i\phi_j dx, \quad C_{ij} = 2v\int_0^1 \phi_i\phi_{j,x}dx \quad \tilde{K}_{ijrg} = -\frac{3}{2}v_1^2\int_0^1 \phi_i\phi_{j,x}\phi_{r,x}\phi_{g,xx}, dx$$

Journal Pre-proof

Journal Pre-proof

$$K_{ij} = (v^2 - 1)\int_0^1 \phi_i \phi_{j,xx} dx + v_f^2 \int_0^1 \phi_i \phi_{j,xxxx} dx,$$

$$\tilde{f}_{ij} = \int_0^1 f \phi_i \phi_j dx, \quad \Omega = \omega \sqrt{\frac{\rho A L^2}{P}}.$$

By restricting the number of transverse degrees of freedom $N = 2$ in the series solution Eq.(15) and Eq.(16), and after introducing weak modal damping μ_{11} and μ_{22}, we obtain the reduced mathematical model of axially moving beam with nonlinear attachment in the following form

$$\ddot{q}_1 + \mu_{11}\dot{q}_1 - \mu_{12}\dot{q}_2 + k_{11}q_1 + k_{12}q_1 q_2^2 + k_{13}q_1^3 + 2k(q_1 - y)^3 + 2b(\dot{q}_1 - \dot{y}) = f_1 \cos(\Omega t), \tag{18}$$

$$\ddot{q}_2 + \mu_{21}\dot{q}_1 + \mu_{22}\dot{q}_2 + k_{21}q_2 + k_{22}q_2 q_1^2 + k_{23}q_2^3 = f_2 \cos(\Omega t), \tag{19}$$

$$\varepsilon \ddot{y} + k(y - q_1)^3 + b(\dot{y} - \dot{q}_1) + \tilde{k}_p y - \tilde{G}Q = 0, \tag{20}$$

$$\tilde{R}\dot{Q} - y + Q = 0, \tag{21}$$

where we defined new parameters as

$$\mu_{12} = \frac{16v}{3}, \quad k_{11} = -\pi^2(v^2 - 1) + \pi^4 v_f^2, \quad k_{12} = 3\pi^4 v_1^2, \quad k_{13} = \frac{3}{8}\pi^4 v_1^2,$$

$$\mu_{21} = \frac{16v}{3}, \quad k_{21} = -4\pi^2(v^2 - 1) + 16\pi^4 v_f^2, \quad k_{22} = 3\pi^4 v_1^2, \quad k_{23} = 6\pi^4 v_1^2.$$

For simplicity, the above equations are derived for the case when the nonlinear attachment is placed at the half of the beam's length i.e. $d = \frac{1}{2}$. However, the proposed methodology gives enough information for accurate modeling of the proposed system where the effects of the nonlinear attachment are given on the frequency response diagrams.

3.2. The incremental harmonic balance method

In order to get the periodic response of the presented system of nonlinear differential equations Eq.(18) - Eq.(21), we will introduce the semi-analytical technique known as the incremental harmonic balance method (IHBM) [48–50]. One of the most important advantages of the IHBM lies in the fact that it can be easily combined with the continuation algorithms for finding the system response for different model parameters. In the following, we will use the IHBM to get the frequency response of the axially moving beam with a NES-EH attachment. The first step in the IHBM is to introduce a new time scale $\tau = \Omega t$ into Eq.(18) - Eq.(21), where we get

$$\Omega^2 \ddot{q}_1 + \mu_{11}\Omega\dot{q}_1 - \mu_{12}\Omega\dot{q}_2 + k_{11}q_1 + k_{12}q_1 q_2^2 + k_{13}q_1^3 + 2k(q_1 - y)^3 + 2b\Omega(\dot{q}_1 - \dot{y}) = f_1 \cos\tau, \tag{22}$$

$$\Omega^2 \ddot{q}_2 + \mu_{21}\Omega\dot{q}_1 + \mu_{22}\Omega\dot{q}_2 + k_{21}q_2 + k_{22}q_2 q_1^2 + k_{23}q_2^3 = f_2 \cos\tau, \tag{23}$$

$$\varepsilon\Omega^2 \ddot{y} + k(y - q_1)^3 + b\Omega(\dot{y} - \dot{q}_1) + \tilde{k}_p y - \tilde{G}Q = 0, \tag{24}$$

$$\tilde{R}\Omega\dot{Q} - y + Q = 0, \tag{25}$$

in which the time derivative $\dot{(\cdot)}$ will be used to represent $\partial(\cdot)/\partial\tau$.

In the second step, we will introduce the incremental relation for generalized coordinates q_1, q_2, y and Q as well as excitation frequency Ω in order to linearize the nonlinear system Eq.(18) - Eq.(21). Here, q_{10}, q_{20}, y_0, Q_0 and Ω_0 represents initial vibration state while increments in their neighborhood are given as

$$q_1 = q_{10} + \Delta q_1, \quad q_2 = q_{20} + \Delta q_2, \quad y = y_0 + \Delta y, \tag{26}$$

$$Q = Q_0 + \Delta Q, \quad \Omega = \Omega_0 + \Delta\Omega.$$

In order to determine periodic solutions of the system Eq.(18) - Eq.(21), we can assume solutions for q_{10}, q_{20}, y_0 and Q_0 and their increments in the form of a finite Fourier series as:

$$q_{10}(\tau) = \sum_{n=1}^{M} [a_{1n}\cos(2n-1)\tau + b_{1n}\sin(2n-1)\tau] = \mathbf{C}\mathbf{A}_1, \tag{27}$$

$$q_{20}(\tau) = \sum_{n=1}^{M} [a_{2n}\cos(2n-1)\tau + b_{2n}\sin(2n-1)\tau] = \mathbf{C}\mathbf{A}_2,$$

$$y_0(\tau) = \sum_{n=1}^{M} [a_{3n}\cos(2n-1)\tau + b_{3n}\sin(2n-1)\tau] = \mathbf{C}\mathbf{A}_3,$$

$$Q_0(\tau) = \sum_{n=1}^{M} [a_{4n}\cos(2n-1)\tau + b_{4n}\sin(2n-1)\tau] = \mathbf{C}\mathbf{A}_4,$$

where

$$\mathbf{C} = [\cos(\tau) \quad \cos(3\tau) \quad \dots \quad \cos(n\tau) \quad \sin(\tau) \quad \sin(3\tau) \quad \dots \quad \sin(n\tau)],$$
$$\mathbf{A}_p = [a_{p1} \quad a_{p3} \quad \dots \quad a_{pn} \quad b_{p1} \quad b_{p3} \quad \dots \quad b_{pn}]^T, (p = 1, ..., 4).$$

and for the increments as

$$\Delta q_1 = \mathbf{C}\Delta\mathbf{A}_1, \quad \Delta q_2 = \mathbf{C}\Delta\mathbf{A}_2, \quad \Delta y = \mathbf{C}\Delta\mathbf{A}_3, \quad \Delta Q = \mathbf{C}\Delta\mathbf{A}_4, \tag{28}$$

where

$$\Delta\mathbf{A}_p = [\Delta a_{p1} \quad \Delta a_{p3} \quad \dots \quad \Delta a_{pn} \quad \Delta b_{p1} \quad \Delta b_{p3} \quad \dots \quad \Delta b_{pn}]^T, (p = 1, ..., 4).$$

Now, by inserting relations Eq.(27) and Eq.(28) into Eq.(26) and applying the Galerkin procedure [48], we can neglect the higher order terms to get the system of algebraic equations as

$$\begin{bmatrix} \mathbf{K}_{11} & \mathbf{K}_{12} & \mathbf{K}_{13} & 0 \\ \mathbf{K}_{21} & \mathbf{K}_{22} & 0 & 0 \\ \mathbf{K}_{31} & 0 & \mathbf{K}_{33} & \mathbf{K}_{34} \\ 0 & 0 & \mathbf{K}_{43} & \mathbf{K}_{44} \end{bmatrix} \begin{Bmatrix} \Delta\mathbf{A}_1 \\ \Delta\mathbf{A}_2 \\ \Delta\mathbf{A}_3 \\ \Delta\mathbf{A}_4 \end{Bmatrix} = \begin{Bmatrix} \tilde{\mathbf{F}}_1 \\ \tilde{\mathbf{F}}_2 \\ 0 \\ 0 \end{Bmatrix} + \begin{Bmatrix} \tilde{\mathbf{R}}_1 \\ \tilde{\mathbf{R}}_2 \\ \tilde{\mathbf{R}}_3 \\ \tilde{\mathbf{R}}_4 \end{Bmatrix} + \begin{Bmatrix} \tilde{\mathbf{V}}_1 \\ \tilde{\mathbf{V}}_2 \\ \tilde{\mathbf{V}}_3 \\ \tilde{\mathbf{V}}_4 \end{Bmatrix} \Delta\Omega, \tag{29}$$

where

$$\tilde{\mathbf{R}}_1 = \mathbf{R}_{11}\mathbf{A}_1 + \mathbf{R}_{12}\mathbf{A}_2 + \mathbf{R}_{13}\mathbf{A}_3, \quad \tilde{\mathbf{R}}_2 = \mathbf{R}_{21}\mathbf{A}_1 + \mathbf{R}_{22}\mathbf{A}_2,$$
$$\tilde{\mathbf{R}}_3 = \mathbf{R}_{31}\mathbf{A}_1 + \mathbf{R}_{33}\mathbf{A}_3 + \mathbf{R}_{34}\mathbf{A}_4, \quad \tilde{\mathbf{R}}_4 = \mathbf{R}_{43}\mathbf{A}_3 + \mathbf{R}_{44}\mathbf{A}_4,$$
$$\tilde{\mathbf{V}}_1 = \mathbf{V}_{11}\mathbf{A}_1 + \mathbf{V}_{12}\mathbf{A}_2 + \mathbf{V}_{13}\mathbf{A}_3, \quad \tilde{\mathbf{V}}_2 = \mathbf{V}_{21}\mathbf{A}_1 + \mathbf{V}_{22}\mathbf{A}_2,$$
$$\tilde{\mathbf{V}}_3 = \mathbf{V}_{31}\mathbf{A}_1 + \mathbf{V}_{33}\mathbf{A}_3, \quad \tilde{\mathbf{V}}_4 = \mathbf{R}_{44}\mathbf{A}_4,$$

in which $\mathbf{K}_{ij}, \mathbf{R}_{ij}$ and $\mathbf{V}_{ij}$ are matrices and $\tilde{\mathbf{F}}_i$ are vectors defined in **Appendix 1**. The Galerkin procedure [48] is introduced in order to eliminate the parameter τ through the orthogonality conditions of the trigonometric functions.

The Eq.(29) can be written in the simplified form as

$$\mathbf{K}\Delta\mathbf{A} = \mathbf{R} + \mathbf{V}\Delta\Omega. \tag{30}$$

If we need just a single frequency response we can introduce $\Delta\Omega = 0$ into the system of linear algebraic equations Eq.(30). In order to solve the system Eq.(30), we start with the solution process by initializing the coefficients $\mathbf{A}$ in such a manner that the tangent stiffens matrix $\mathbf{K}$ is not a singular matrix. Then, by using the Newton âĂŞ Raphson iterative procedure we find the solution of $\Delta\mathbf{A}$ iteratively by solving

$$\Delta\mathbf{A} = \mathbf{K}^{-1}\mathbf{R} \quad \longrightarrow \quad \mathbf{A}_{i+1} = \mathbf{A}_i + \Delta\mathbf{A}_{i+1}, \tag{31}$$

The iterations are performed until the residue Euclidian norm $\|\mathbf{R}\|$ is smaller than a pre-set tolerance (we adopt $\zeta = 10^{-12}$).

It is important to note that the corrective vector term $\mathbf{R}$ tends to zero when the values of coordinates tend to the exact solutions. In order to determine amplitude - frequency responses of the system, the value of Ω should increase with increment $\Delta\Omega$ and the solution of $\mathbf{A}$ at the previous frequency step is used as the initial guess for finding the solution for the current frequency. Better accuracy is achieved for smaller increments $\Delta\Omega$.

Journal Pre-proof

Journal Pre-proof

4. The continuation method

The drawback of the previously described procedure for simple incrementation of the excitation frequency $\Delta\Omega$ in the process of obtaining the frequency response curves lies in the fact that a frequency response reaches certain limit points (such as turning points) or solution curves are obtained in the form of loops, where the tangent stiffens matrix $\mathbf{K}$ becomes a singular matrix. In such cases, the previously described simple incremental procedure fails. In order to avoid such cases and to eliminate failures due to the limit points, we will introduce a numerical continuation method [51, 52] known as the pseudo-arc-length continuation technique, which traces out periodic solution branches of the proposed nonlinear system in the form of an amplitude-frequency response. The solution process starts from an arbitrary initial state (e.g. linear solution far away from the resonance state). Then, a point-to-point calculation is performed by using the predictor-corrector methodology to obtain the corresponding response curves as shown in [44, 50, 51].

At the beginning of the tracing process, the incremental relation given in Eq.(30) is used to determine two initial periodic solutions that are far away from the resonant state. Afterwards, we extend the IHBM with augmented equation and the predictor-corrector methodology. One of the most used continuation approaches is the pseudo-arc-length continuation method, which is able to track possible solutions including the limit points and loops. By introducing the parameter η, the augmented equation is given as

$$g(\mathbf{X}) - \eta = 0, \tag{32}$$

where $\mathbf{X} = [\mathbf{A}, \Omega]^T$. By using the quadratic form of the pseudo arc-length continuation approach, as shown in [50, 51], we adopt the following augmented equation

$$g(\mathbf{X}) - \eta = \mathbf{X'}^T(\mathbf{X} - \mathbf{X}_{k-1}) - \eta = 0, \tag{33}$$

where the slope is defined in terms of the two previous points $\mathbf{X}_{k-1}$ and $\mathbf{X}_{k-2}$ on the response curves, and it is given as

$$\mathbf{X}' = \frac{\mathbf{X}_{k-1} - \mathbf{X}_{k-2}}{\|\mathbf{X}_{k-1} - \mathbf{X}_{k-2}\|}. \tag{34}$$

The first predicted solution is calculated based on the first two periodic solutions obtained from IHBM

$$\mathbf{X}_u = \mathbf{X}_{k-1} + \Delta\eta\mathbf{X}'. \tag{35}$$

In order to obtain the periodic solution, we will extend the tangent stiffness matrix by introducing the augmenting equation and then applying the Newton-Raphson iterative procedure for the corrected solution. By combining Eq.(30) and Eq.(33), the extended tangent stiffness matrix can be obtained in the following form

$$\begin{bmatrix} \mathbf{K} & \mathbf{V} \\ \frac{\partial g}{\partial \mathbf{A}} & \frac{\partial g}{\partial \Omega} \end{bmatrix} \begin{Bmatrix} \Delta\mathbf{A} \\ \Delta\Omega \end{Bmatrix} = \begin{Bmatrix} \mathbf{R} \\ \Delta\eta - g \end{Bmatrix}. \tag{36}$$

For more details reffer to the following literature [50, 51].

It is important to note that further points are calculated by updating the values of X' while the value of parameter η is considered to be zero. The parameter $\Delta\eta$ is adopted as the arc increment having a small value. In the literature, one can find more details on how to set the values of the parameter $\Delta\eta$ [52]. In order to determine the periodic responses of the axially moving beam with nonlinear attachments, it is important to set the initial step size of the excitation frequency and tolerance which is related to the degree of nonlinearity and other material parameters of the system. For higher accuracy of periodic solutions, we introduced the tolerance of the order $\zeta = 10^{-10}$ which can go up to $\zeta = 10^{-16}$. Setting small enough tolerances leads to amplitude-frequency solutions without any breaks in the simulation process.

5. Stability analysis of periodic solution

By considering the Floquet stability theory and the Hsu procedures developed in [44, 53, 54], stability of a periodic solution of the axially moving beam with NES-EH attachment will be determined. Inserting small perturbations $\Delta\mathbf{y}(\tau)$ in the neighborhood of a periodic solution $\mathbf{y}_0(\tau)$, i.e. by letting

$$\mathbf{y} = \mathbf{y}_0 + \Delta\mathbf{y}(\tau), \tag{37}$$

Journal Pre-proof

the stability of the periodic solution can be analyzed by introducing the linearized system of differential equations with variable coefficients in terms of small perturbations $\Delta\mathbf{y}(\tau)$. Applying the Floquet theory in $\mathbb{R}^N$, the system of nonlinear differential equations in the general form can be written as

$$\mathbf{W}(\mathbf{y}, \dot{\mathbf{y}}, \ddot{\mathbf{y}}, \tau) = \mathbf{0}, \tag{38}$$

where $\mathbf{y} = [y_1(\tau),\ y_2(\tau), \ldots y_N(\tau)]$ is the N - dimensional displacement vector and $\dot{\mathbf{y}} = d\mathbf{y}/d\tau$. Inserting Eq.(37) into Eq.(38), and after performing linearization, one can obtain the system of linear differential equations with time dependent coefficients as

$$\left(\frac{\partial \mathbf{W}}{\partial \ddot{\mathbf{y}}}\right)_0 \Delta\ddot{\mathbf{y}}(\tau) + \left(\frac{\partial \mathbf{W}}{\partial \dot{\mathbf{y}}}\right)_0 \Delta\dot{\mathbf{y}}(\tau) + \left(\frac{\partial \mathbf{W}}{\partial \mathbf{y}}\right)_0 \Delta\mathbf{y}(\tau) = \mathbf{0}, \tag{39}$$

in which $\mathbf{y}_0(\tau) = [q_{10}(\tau), q_{20}(\tau), y_0(\tau), Q_0(\tau)]^T$ is the periodic solution determined by the IHB procedure. It should be noted that Eq.(39) represents the system of perturbed equations in the vicinity of the known periodic solutions $\mathbf{y}_0(\tau)$. The stability properties of the determined periodic solutions are found through the Hsu procedures given in [53, 54]. Transformation of Eq.(39) into the state-space form yields

$$\frac{d\mathbf{Y}}{d\tau} = \mathbf{P}(\tau)\,\mathbf{Y}, \tag{40}$$

where $\mathbf{Y}(\tau) = [\Delta\mathbf{y}, \Delta\dot{\mathbf{y}}]^T$ and $\mathbf{P}(\tau)$ denotes the periodic matrix with the period T. The stability criteria based on the Floquet theory [52, 55] for determination of the stability property of the periodic solutions Eq.(27) is based on solving the eigenvalues of the monodromy matrix i.e. Floquet multipliers. In the case where all values of Floquet multipliers are located inside the unit circle centered at the origin of the complex plane, the periodic solutions are stable or asymptotically stable. On the other hand, when the Floquet multipliers lie outside of the unit circle in the complex plane, the periodic solutions are unstable [52, 55]. The stability of the periodic solutions, depending on a location where the Floquet multipliers or a pair of complex conjugate multipliers crosses the unit circle, one can detect different bifurcation points such as Hopf, Saddle-node, and period of doubling bifurcations [52, 55]. In the following, it is assumed that the period $T = 2\pi$ of $y_0(\tau)$ is divided into N_k sub-intervals, in which the k-th interval is $\Delta_k = \tau_k - \tau_{k-1}$ for $\tau_k = kT/N_k$. In the case when the $P(\tau)$ is the continuous periodic matrix with respect to τ, such that it can be replaced by a constant matrix in the k-th interval for the case when N_k is chosen to be sufficiently large, as

$$\mathbf{P}_k = \frac{1}{\Delta_k}\int_{\tau_{k-1}}^{\tau_k} \mathbf{P}(\tau)\, d\tau, \tag{41}$$

where the transition matrix can take the following form

$$\mathbf{M} = \prod_{i=1}^{N_k} e^{\mathbf{P}_i \Delta_i} = \prod_{i=1}^{N_k}\left(\mathbf{I} + \sum_{j=1}^{N_j} \frac{(\mathbf{P}_i\Delta_i)^j}{j!}\right), \tag{42}$$

in which N_j denotes the number of terms in the approximation of the constant matrix $\mathbf{P}_k$. From the transition matrix $\mathbf{M}$ one can obtain Floquet multipliers as eigenvalues of Eq.(42) in the form

$$\det(\mathbf{M} - \sigma\ \mathbf{I}) = 0. \tag{43}$$

6. Numerical results

In this Section, the previously presented methodology based on IHB, the continuation technique and the Floquet stability theory is used to determine the stable and unstable branches of the periodic responses of the axially moving beam with coupled NES-EH attachment. The amplitude-frequency response diagrams are used to investigate the effects of the transporting speed as well as the presence of the nonlinear attachment on the dynamic behavior of the axially moving beam. For better understanding of the effect of nonlinear attachment, this section will be divided into two parts. In the first part, the axially moving beam with and without the attachments is analyzed for different values of transporting speed v and the obtained results are compared with the results from the literature [44]. Afterwards, a detailed analyses of the effect of axially transporting speed and transverse load on the periodic response will be shown. In the second part, we will present the frequency and time response diagrams, where the effects of energy transfer and dissipation

Journal Pre-proof

through nonlinear attachment will be studied. It should be noted that all the system parameters given in ***Appendix 1*** are first determined in the symbolic form and then introduced into the IHB code developed in the Matlab software. We define the response amplitudes from Eq.(27) as

$$q_1(\tau) = A_{11}\cos(\tau+\phi_{11}) + A_{12}\cos(3\tau+\phi_{12}) + ..., \tag{44}$$

$$q_2(\tau) = A_{21}\cos(\tau+\phi_{21}) + A_{22}\cos(3\tau+\phi_{22}) + ...,$$
$$y(\tau) = A_{31}\cos(\tau+\phi_{31}) + A_{32}\cos(3\tau+\phi_{32}) + ...,$$
$$Q(\tau) = A_{41}\cos(\tau+\phi_{41}) + A_{42}\cos(3\tau+\phi_{42}) + ...,$$

where

$$A_{jk} = \sqrt{a_{ij}^2 + b_{jk}^2}, \quad \phi_{jk} = \tan^{-1}(b_{jk}/a_{ij}), \quad j = 1, ..., 4 \quad k = 1, ..., 5.$$

The system parameters of the presented axially moving beam are adopted from [56], where the value of the axial transporting speed is adopted as $v = \{0.2, 0.4, 0.6, 0.8\}$.

When considering the nonlinear problem of the axially moving beam, where the cubic nonlinearity plays an important role in the discretized model, three to one internal resonance can be observed. Starting from the discretized equations Eq.(18) - Eq.(21), and neglecting the external damping parameters (μ_{11}, μ_{22}), the characteristic equation for the linear system of axially moving beam takes the following form

$$\omega^4 - (k_{11} + k_{21} + \mu_{12}\mu_{21})\omega^2 + k_{11}k_{22} = 0. \tag{45}$$

The characteristic equation is solved for $v = 0.6$ with the following values of natural frequencies $\omega_1 = 2.8223$ and $\omega_2 = 9.1398$. In the nonlinear system with cubic nonlinearity, the phenomenon known as internal resonance occurs between modes when $\omega_2 \approx 3\omega_1$.

6.1. Comparative study

In order to validate the extended model of axially moving beam with nonlinear attachments, the IHB, continuation method and Floquet stability theory are used to trace the periodic responses and determine their stability for different values of transporting speed v. It should be noted that the results obtained in [44] are presented only for the values of transporting speed $v = 0.6$ and the amplitude of excitation load $f_1 = 0.0055$. However, in this paper, we extend the parametric analyses to different values of transporting speed $v = \{0.2, 0.4, 0.6, 0.8\}$ and higher values of excitation load amplitude $f_1 = 0.0077$. The nonlinear phenomenon known as nonlinear "hysteresis", with coexisting periodic orbits, is detected on the amplitude-frequency response diagrams. For the solution process, the first five odd terms in the Fourier series $(M = 5)$ are adopted in Eq.(27) and Eq.(28). The Hsu procedure is adopted for approximation of the transition matrix to analyze the stability of periodic solutions. Based on the convergence study given in [57], the transition matrix is determined by adopting the following values of parameters: $N_k = 5000$ and $N_j = 5$.

Fig.2 shows the effect of different values of transporting speed $v = \{0.2, 0.4, 0.6, 0.8\}$ on the amplitude-frequency response for the case of an axially moving beam without a nonlinear attachment. The ordinate axis represents the amplitudes A_{11} and A_{22} of the two most influenced modes of both displacements, while the abscissa shows frequency ratio Ω/ω_1. For the complete analysis of the amplitude-frequency response, branches of stable and unstable periodic solutions are determined based on the Floquet stability theory. The blue solid line represents stable periodic solutions while red point branches represents unstable periodic solutions. Both amplitude-frequency responses, A_{11} and A_{22}, show a nonlinear "hysteresis" part of the response with coexisting multiple periodic solutions. Forward frequency sweeping, for which the frequency ratio increases Ω/ω_1 starting from some small value $(\Omega/\omega_1 = 0.6)$, leads to an increase of both amplitudes A_{11} and $A22$ until Ω/ω_1 reaches the value where the periodic solution loses its stability due to the appearance of a saddle-node bifurcation. This instability is detected by the calculation of Floquet multipliers, where at least one of them crosses the unit circle in the complex plane in $+1$ direction. Further increase in the frequency ratio Ω/ω_1 leads to the "jump-down" effect, i.e. a dramatic decrease in the values of the response amplitude. On the other hand, the backward frequency sweeping will start from some higher values of the frequency ratio $(\Omega/\omega_1 = 2)$ and decrease while the response amplitude slowly increases. However, when the frequency ratio reaches the value where the periodic solution loses its stability, the "jump-up" phenomena will appear and the response amplitude will increase. This process of forward and backward frequency sweeping results in a generation of the aforementioned "hysteresis" phenomenon with coexisting periodic solutions. For the values of transporting speed $v = 0.6$, the 3:1 internal resonance can be detected (Fig.2) since the natural

Journal Pre-proof

frequencies ω_2 and ω_1 are commensurable in ratio $\omega_2 \approx 3\omega_1$. From the physical point of view, the natural frequencies of the axially moving beam are directly dependent on the transporting speed v. Further increase of the transporting speed until the value $v = 0.8$ results in increased values of the response amplitude, when the nonlinear hysteresis phenomenon becomes more prominent.

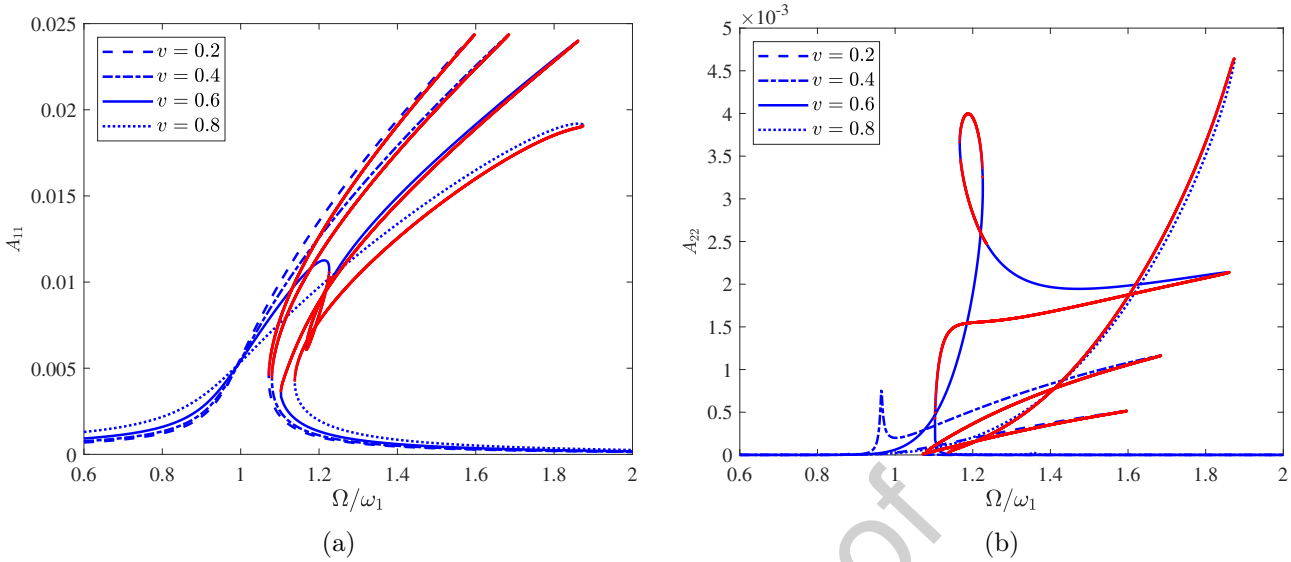

Figure 2: The amplitude-frequency response curves of the axially moving beam for different values of transporting speed v and the excitation load amplitude $f_1 = 0.0055$. Blue solid lines represent stable branches, while the red dotted lines represent unstable branches of the amplitude-frequency response curves. The response amplitude A_{11}, given in the sub-figure a), and response amplitude A_{22}, given in the sub-figure b), are defined in Eq.(44).

Fig. 3 shows the amplitude-frequency responses of the axially moving beam without the external nonlinear attachment, influenced by the higher values of excitation load amplitude $f_1 = 0.0077$, varying transporting speed v and obtained for the frequency ratio Ω/ω_1 within the range $0.6-2.5$. The frequency response diagrams for amplitudes A_{11} and A_{22} shown in Fig.3 exhibit nonlinear hysteresis phenomenon showing coexisting multiple periodic solutions. The stable and unstable branches of the periodic solutions are displaying similar properties, as in the previous case. However, an increase of the transporting speed can cause widening of unstable branches. Moreover, by comparing the amplitudes given in Fig. 2 and Fig. 3, it can be concluded that an increase of the values of excitation load amplitude increases the magnitudes of response amplitudes, which leads to an extended frequency range in which the "hysteresis" appears in the amplitude-frequency response for all the values of transporting speed v. It should be noted that there are significant differences in the response amplitudes for the cases with lower and higher values of excitation load f_1 when the transporting speed is equal to $v = 0.6$. However, these changes are obvious when the axially transporting speed reaches the value $v = 0.8$, since the response amplitude A_{11} significantly decreases while the amplitude A_{22} becomes larger.

Further, Fig.4 and Fig.5 show the effects of a NES attachment on vibration amplitudes of the axially moving beam. Here, the response diagrams are determined for the values of excitation load $f_1 = 0.0055$ and $f_1 = 0.0077$, respectively. Comparing the amplitudes (A_{11} and A_{22}), one can notice a significant reduction of their magnitudes due to the introduced NES device. Moreover, both stable and unstable branches of the periodic solution are determined, where the blue solid lines represent stable branches, while the red points represent unstable branches of the periodic responses. It can be observed that the introduced NES device leads to a decrease in vibration response amplitudes more than 50% of the initial vibration amplitudes of the pristine axially moving beam. An interesting behavior can be noticed for the case with excitation load $f_1 = 0.0055$, where the response amplitude A_{11} loop vanishes (Fig.4) while in the case of $f_1 = 0.0077$ a loop appears again. By analyzing the response amplitudes A_{11} and A_{22} for $v = 0.6$, it can be observed that the energy transfer occurs between the first and the second vibration mode through the internal resonance phenomena. The material parameters used in this case for tracing the frequency response diagrams are: $k = 50$, $b = 0.05$, $\tilde{k}_p = 3$, $\epsilon = 0.1$.

Validation of the proposed solution

In order to show the correctness of the presented methodology for solving the coupled system of nonlinear differential equations, the approximate results obtained by the IHB method are compared with the results

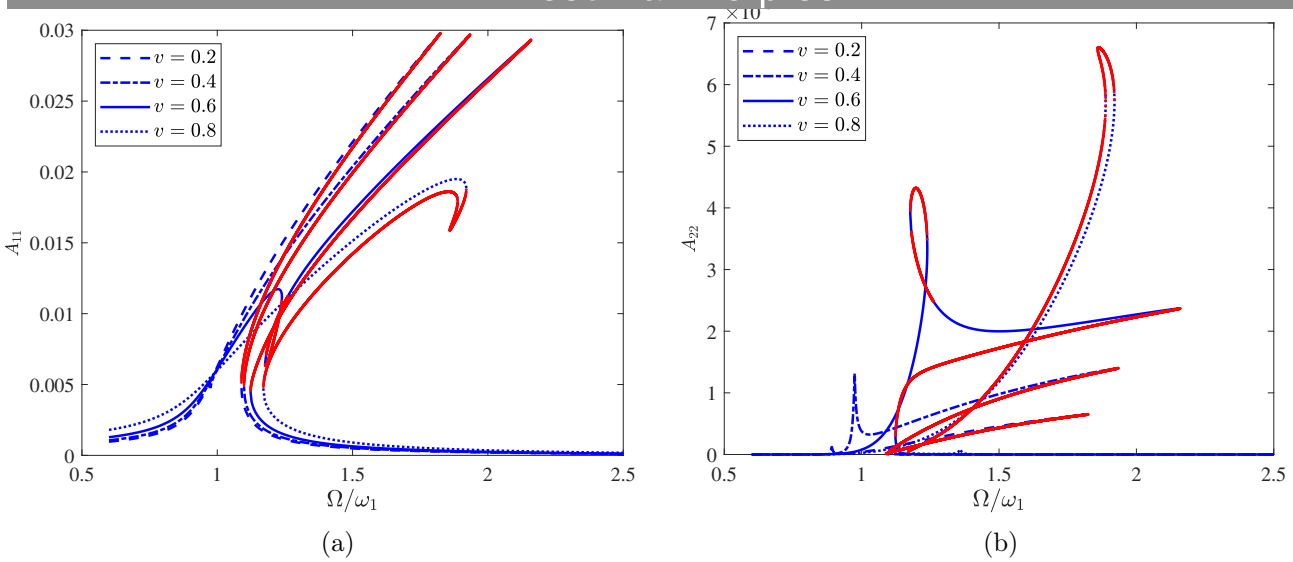

Figure 3: The amplitude-frequency response curves of the axially moving beam for different values of transporting speed v and excitation load amplitude $f_1 = 0.0077$. The blue solid lines represent the stable branches, while the red dotted lines represent the unstable branches of the amplitude-frequency response curves. The response amplitude A_{11}, given in the sub-figure a), and the response amplitude A_{22}, given in the sub-figure b), are defined in Eq.(44).

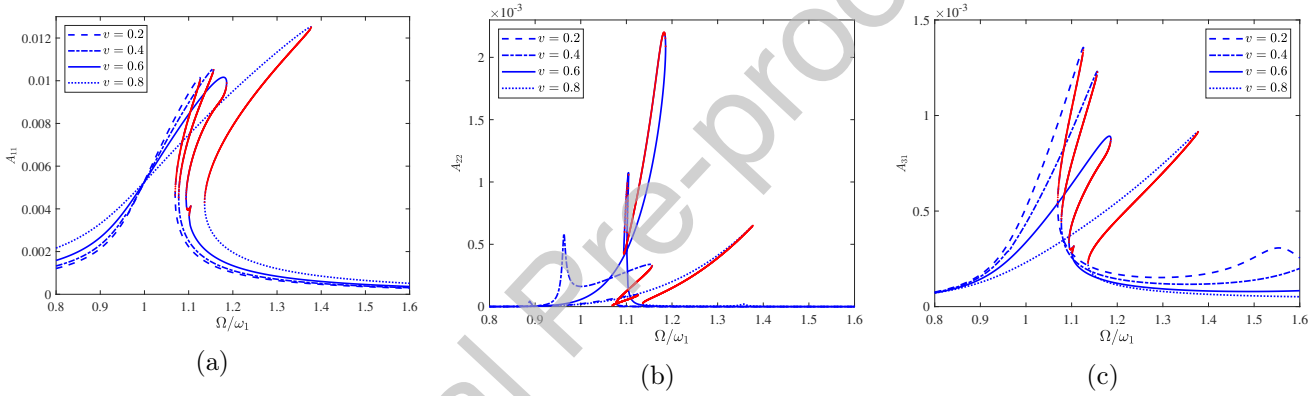

Figure 4: The amplitude-frequency response curves A_{11}, A_{22} and A_{31} of the axially moving beam with the NES device. The blue solid lines represent stable branches, while the red dotted lines represent unstable branches on the frequency response diagrams. The response curves A_{11}, A_{22} and A_{31} are given in sub-figures a), b) and c), respectively, for the excitation load amplitude $f_1 = 0.0055$.

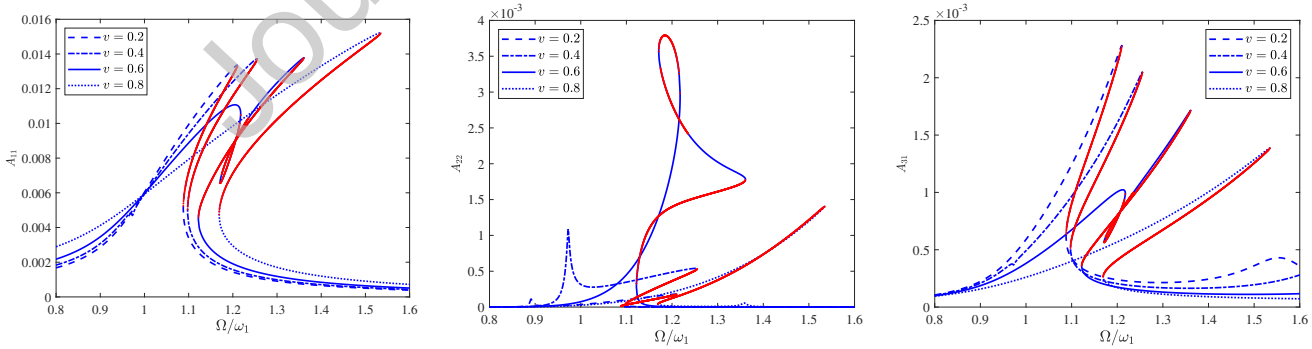

Figure 5: The amplitude-frequency response curves A_{11}, A_{22} and A_{31} of the axially moving beam with the NES device. The blue solid lines represent stable branches, while the red dotted lines represent unstable branches of the amplitude-frequency response curves. The response curves A_{11}, A_{22} and A_{31} are given in a), b) and c), respectively for the excitation load amplitude $f_1 = 0.0077$.

obtained by the Runge-Kutta method (*ode*45 in Matlab). The periodic solutions are depicted in the phase plane, where the velocity is given on the ordinate axis while the displacement is on the abscissa. Fig.6 shows periodic solutions determined by solving Eq.(22) - Eq.(25), where the blue solid line represents the

Journal Pre-proof

solution determined by the IHB method while the "red circles" correspond to the periodic solutions found by direct numerical integration. It can be noticed that the periodic solutions obtained by the approximate IHB method are in good agreement with those obtained by the numerical integration method. The following dimensionless parameters are adopted in this analysis: $v = 0.6$, $f_1 = 0.07$, $k = 10$, $b = 0.05$, $\tilde{k}_p = 3$, $\epsilon = 0.1$, $\tilde{G} = 5$, $\tilde{R} = 1$, $\Omega = 0.9\omega_1$. Values of other system parameters are adopted from [44]. The initial conditions used in the numerical calculation are generated by the periodic solution obtained from the IHB method when setting $\tau = 0$.

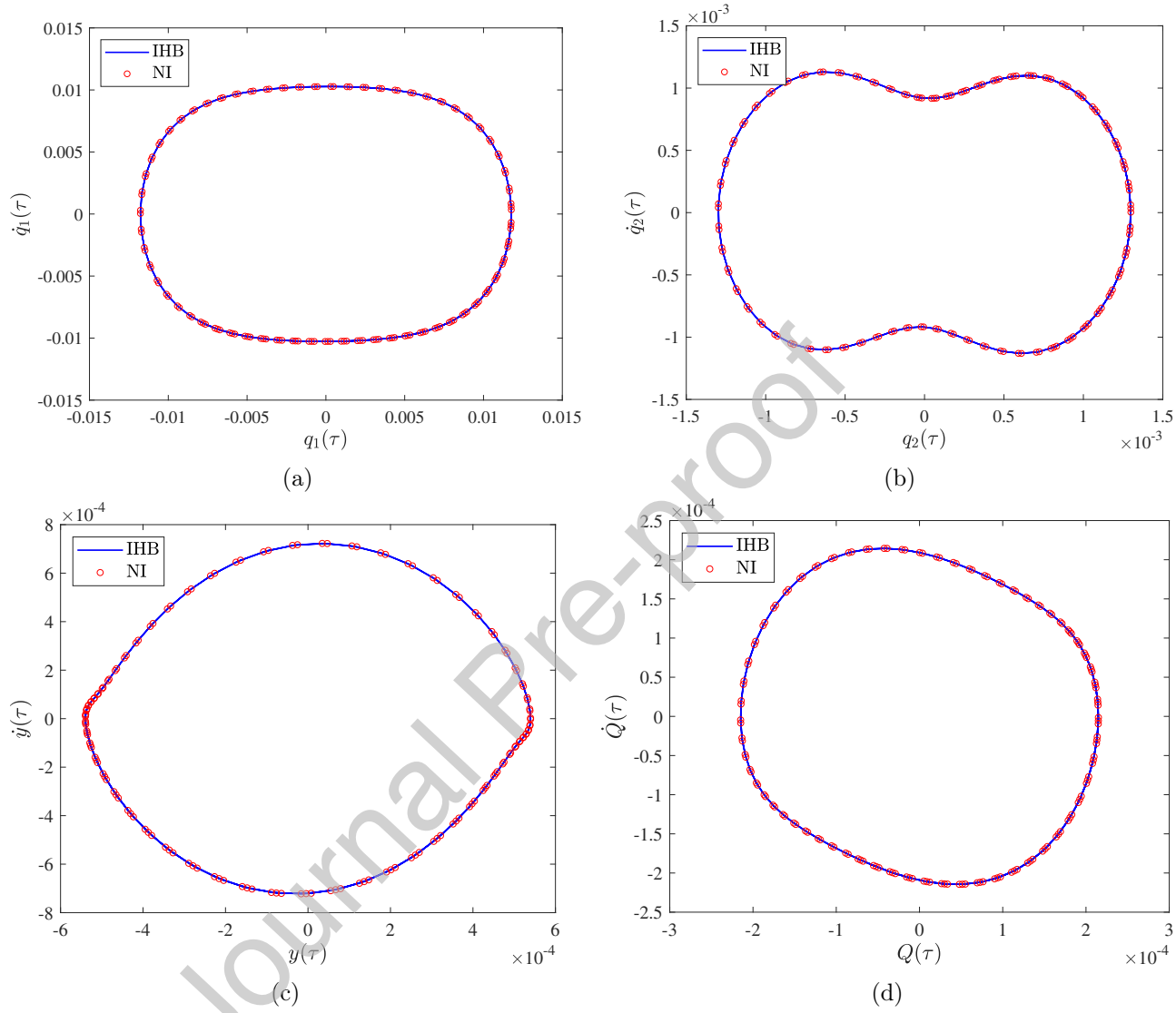

Figure 6: The periodic solutions obtained by the incremental harmonic balance (IHB) method and direct numerical integration (NI) depicted in the phase plane. The results obtained with the IHB method are represented by the blue solid lines while the results obtained b direct NI are represented by the red circles.

6.2. Parametric study

Here, we investigate how the transporting speed v, linear stiffness parameter $\tilde{k}_p$, and excitation load amplitude f_1, affect the amplitude-frequency responses for amplitudes A_{11}, A_{22}, A_{31} and A_{41} of the presented axially moving beam model with a NES-EH device attached. The response amplitudes A_{11}, A_{22}, A_{31} are the amplitudes of the mechanical displacements and A_{41} corresponds to the output electrical charge, defined in Eq.(44). The particular cases of the excitation load amplitude are adopted as lower $f_1 = 0.0055$, $f_1 = 0.0077$ and higher $f_1 = 0.07$ values, for which significant changes of the amplitudes can be observed. Moreover, different qualitative behavior of the frequency responses can be noticed for the moving beam with NES-EH device presented in Figs. 7 - 11. The frequency ratio Ω/ω_1 is varied in the range $0.6 - 2$ for lower load values, and in the range $\Omega/\omega_1 = 0.6 - 4.5$ for higher values of the excitation load .

Fig. 7 shows the amplitude-frequency responses for the amplitude A_{11} of the axially moving beam with NES-EH and different values of transporting speed v, linear stiffness $\tilde{k}_p$ and excitation load f_1. Starting

Journal Pre-proof

from some small value of the frequency ratio $\Omega/\omega_1 = 0.6$, which is far from the resonance state, a continuous increase of its value increases the response amplitude A_{11} until the frequency ratio parameter reaches a peak value where the periodic solution loses its stability. Amplitude A_{11} is very sensitive to changes in the frequency ratio Ω/ω_1, where small increase in this parameter results in a significant decrease of the amplitude. It should be noted that for all values of transporting speed v we have similar behavior of the frequency response curves with a pronounced stiffness hardening effect. Moreover, variation of the linear stiffness parameter $\tilde{k}_p$ causes small changes of the amplitude A_{11}. However, in the case when the transporting speed is $v = 0.6$ and excitation load $f_1 = 0.0077$, the response curve forms a loop where two peak amplitudes can be observed, represented by the blue solid line on 7 (c) and (d).

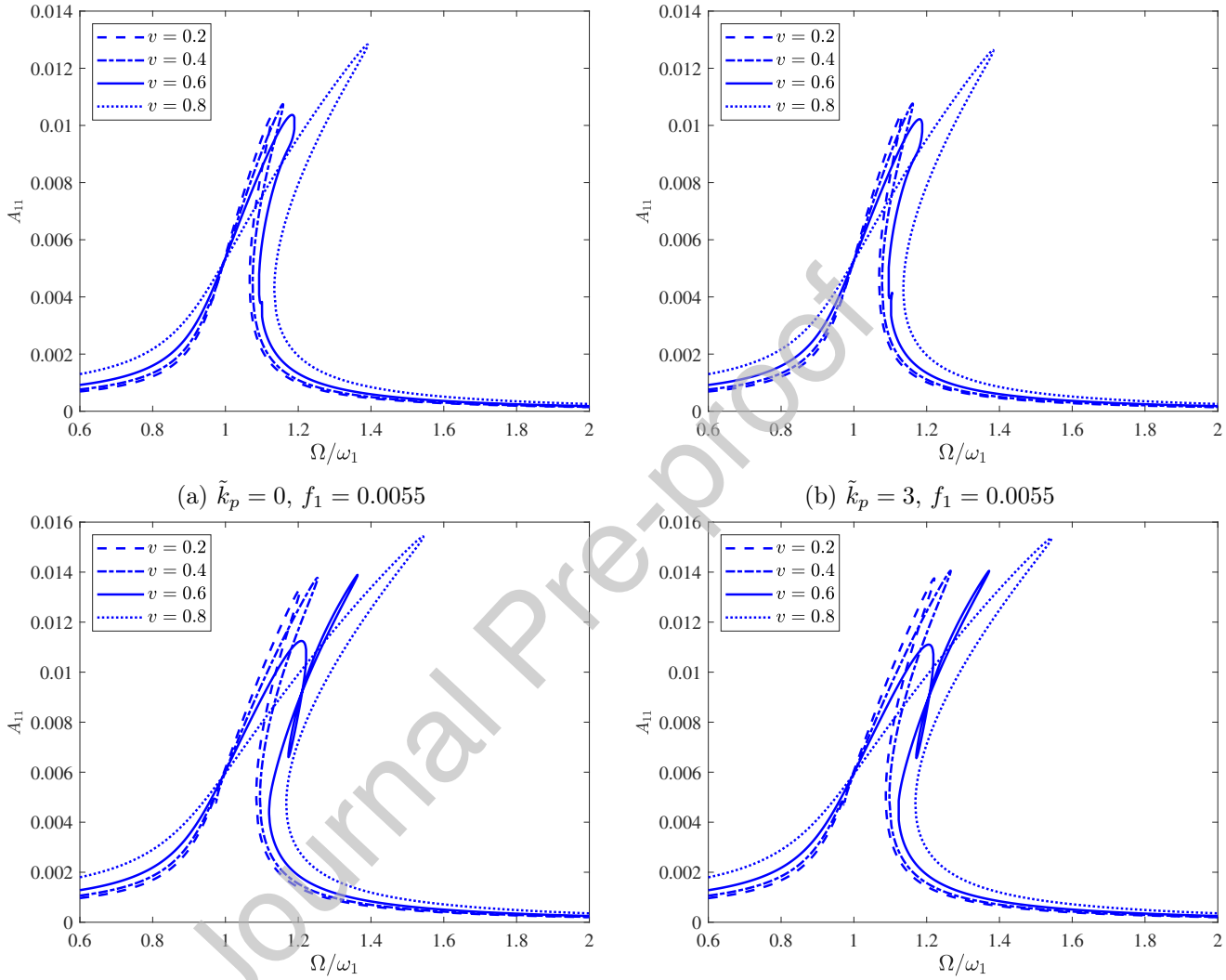

(a) $\tilde{k}_p = 0,\ f_1 = 0.0055$ (b) $\tilde{k}_p = 3,\ f_1 = 0.0055$

(c) $\tilde{k}_p = 0,\ f_1 = 0.0077$ (d) $\tilde{k}_p = 3,\ f_1 = 0.0077$

Figure 7: The amplitude-frequency response curves A_{11} of the axially moving beam with nonlinear NES-EH attachment for different values of transporting speed v, and linear stiffness parameter $\tilde{k}_p$.

Figure 8 shows the amplitude-response curves for the amplitude A_{22} determined for the axially moving beam with an NES-EH attached, for different values of linear stiffness parameter $\tilde{k}_p$, transporting speed v and excitation load f_1. It can be observed that an increase of the transporting speed v from the value 0.2 to some higher values causes a significant and qualitative changes in the amplitude-frequency response curves near the resonance state. The value of the response amplitude A_{22} is the biggest for the case when transporting speed is equal to $v = 0.6$. Further, an increase of the value of linear stiffness parameter $\tilde{k}_p$ for a fixed value of transporting speed $v = 0.6$ leads to an increase of the area with coexisting periodic solutions, where the response curve forms a loop. Similar behavior can be noticed in Fig.7, where the amplitude A_{11} has a local minimum. A detailed analysis of the response amplitudes A_{11} and A_{22} shows energy transfer between the first two vibration modes that is caused by the internal resonance phenomena when $\omega_2 \approx 3\omega_1$. Moreover, one can notice a weak influence of parameter $\tilde{k}_p$ on the internal resonance and mode interactions. On the other hand, the effect of the excitation load on the response amplitude A_{22} reflects in an increase of

Journal Pre-proof

the nonlinear hysteresis region with coexisting periodic solutions.

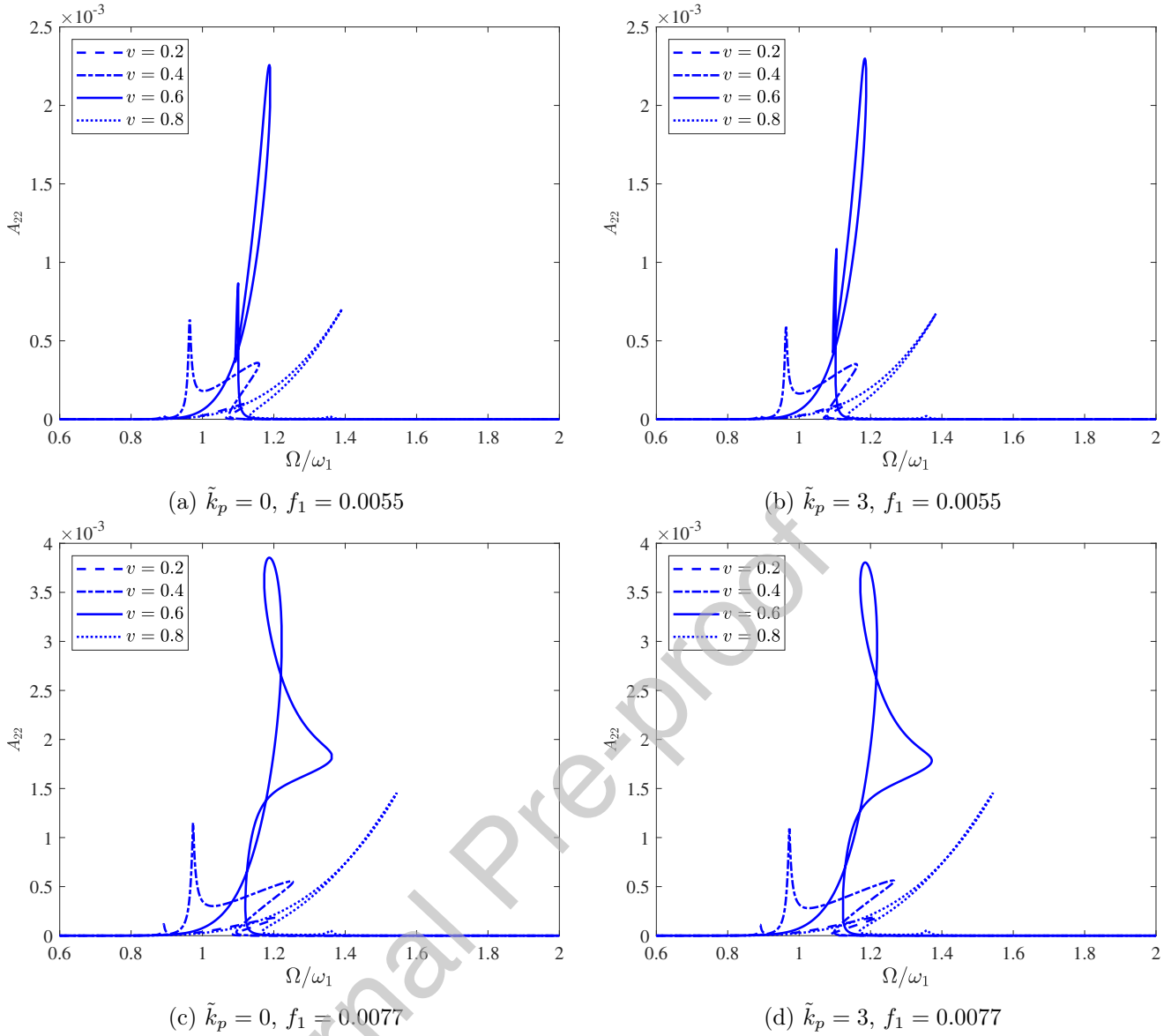

(a) $\tilde{k}_p = 0,\ f_1 = 0.0055$ (b) $\tilde{k}_p = 3,\ f_1 = 0.0055$

(c) $\tilde{k}_p = 0,\ f_1 = 0.0077$ (d) $\tilde{k}_p = 3,\ f_1 = 0.0077$

Figure 8: The amplitude-frequency response curves A_{22} of the axially moving beam with nonlinear NES-EH attachments for different values of transporting speed v and linear stiffness parameter $\tilde{k}_p$.

Figure 9 shows traced amplitude-frequency curves of the amplitude A_{31} for different values of transporting speed v and linear stiffness parameter $\tilde{k}_p$. One can observe similar frequency responses like in the case of the amplitude A_{11}. However, there are some obvious differences, especially for the value of the linear stiffness parameter equal to $\tilde{k}_p = 3$. One can notice that an increase of transporting speed decreases the response amplitude A_{31}, where the hardening nonlinearity is displayed. However, when the liner stiffness parameter is equal to $\tilde{k}_p = 0$, the transporting speed has a similar influence on the response amplitude A_{31}, as shown in Fig. 7. In general, a significant reduction of amplitudes A_{11} and A_{22} by attaching the EH-NES can be observed, where a significant increase of the response amplitude A_{31} indicates that a large amount of mechanical energy is transferred to the nonlinear attachment. This implies that the main goal of attaching the NES-EH device on the axially moving beam is fulfilled.

Figure 10 shows the results for the response amplitude A_{41}, corresponding to the electrical degree of freedom, in the case of the axially moving beam system with NES-EH attachment. Here we analyses the model with lower $f_1 = 0.0055$ and higher values $f_2 = 0.0077$ of the external load amplitude. In Fig.10, it can be noticed that for lower values of external load amplitude $f_1 = 0.0055$ the response amplitude A_{41} increases for an increase of the transporting speed v. However, for the higher values of excitation load $f_1 = 0.0077$, there are no significant changes in the peak value of the response amplitude A_{41} while the interval with multiple periodic orbits is increased for an increase of the transporting speed v. On the other hand, an increase of the linear stiffness parameter $\tilde{k}_p$ implies reduced response amplitudes, as shown in Fig.10(b).

Journal Pre-proof

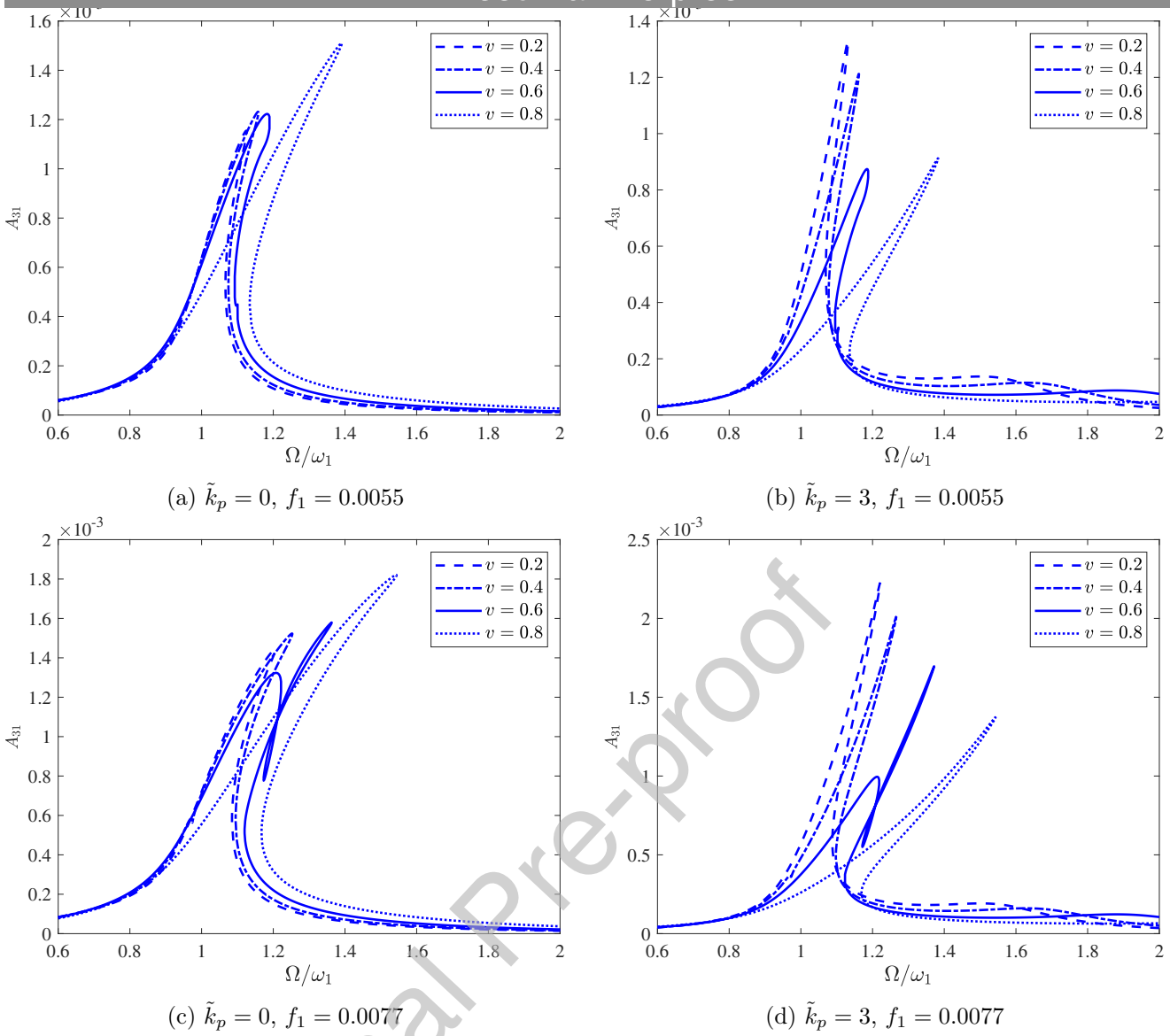

(a) $\tilde{k}_p = 0,\ f_1 = 0.0055$ (b) $\tilde{k}_p = 3,\ f_1 = 0.0055$

(c) $\tilde{k}_p = 0,\ f_1 = 0.0077$ (d) $\tilde{k}_p = 3,\ f_1 = 0.0077$

Figure 9: The amplitude-frequency response curves A_{31} of the axially moving beam with nonlinear NES-EH attachment for different values of transporting speed v and linear stiffness parameter $\tilde{k}_p$.

Based on the previous, it can be concluded that the presented system can harvest more energy for larger transporting speed and external load amplitude.

The influence of higher values of the excitation load amplitude on the amplitude-frequency response curves A_{11}, A_{22} and A_{31} of the axially moving beam with the attached NES-EH device is presented in Fig. 11. The following values of material parameter values are adopted: linear stiffness parameter $\tilde{k}_p = 3$, excitation load amplitude $f_1 = 0.07$, electro-mechanical coupling $\tilde{G} = 4$ and $\tilde{R} = 2$. It can be observed that higher values of the excitation load lead to a significant change in the frequency response curves. By tracing the response curves, starting from $\Omega/\omega_1 = 0.8$, the values of the response amplitude A_{11} increase and create a loop, while for further increase of its value the frequency response curve reaches the turning point. After reaching its peak value, for further increase of the frequency ratio one can observe a decrease of the response amplitude A_{11}. However, an increase of the transporting speed v causes that the hardening stiffness nonlinearity effect. The maximum response amplitude value remains the same for all three analyzed cases. Nevertheless, an increase of the transporting speed v leads to an increase of the maximum value of the response amplitude A_{22} and a widening of the loop (interval with multiple periodic solutions). Comparing the amplitude-frequency response curves for A_{22}, $f_1 = 0.0055$ (Fig. 8) and $f_1 = 0.07$ (Fig.11), a significant difference between these two cases can be observed. In the case of the response amplitudes A_{31} and A_{41}, one can notice a softening stiffness nonlinearity effect. The major consequence of increasing the external load amplitude $f_1 = 0.07$ are much higher response amplitudes, as shown in Fig. 11.

Journal Pre-proof

Journal Pre-proof

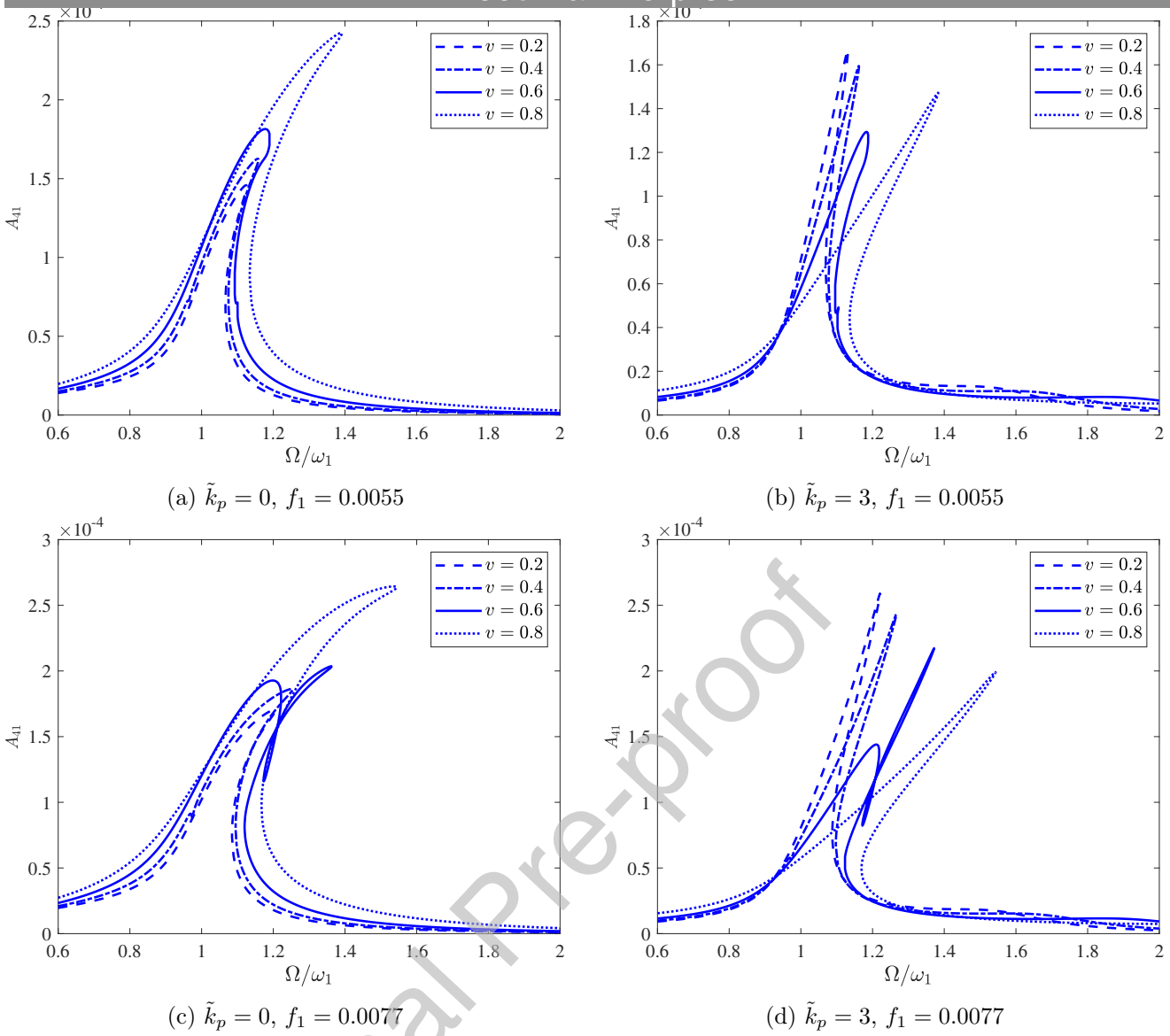

(a) $\tilde{k}_p = 0,\ f_1 = 0.0055$ (b) $\tilde{k}_p = 3,\ f_1 = 0.0055$

(c) $\tilde{k}_p = 0,\ f_1 = 0.0077$ (d) $\tilde{k}_p = 3,\ f_1 = 0.0077$

Figure 10: The amplitude-frequency response curves A_{41} of the axially moving beam with nonlinear NES-EH attachment for different values of transporting speed v, and linear stiffness parameter $\tilde{k}_p$.

6.3. Time response diagrams

To investigate performances of the presented model of an axially moving beam with an attached NES-EH device in the sense of vibration suppression and energy harvesting, the corresponding time response diagrams are presented in Figs.12 - 15. The material parameters used in this analysis are: $f_1 = 0.0055$, $k = 10$, $b = 0.5$, $\tilde{k}_p = 5$, $\epsilon = 0.1$, $\tilde{G} = 3$, $\tilde{R} = 1$, $\Omega = 0.95\omega_1$. The initial conditions are adopted as $q_1(0) = 0.03$, $\dot{q}_1(0) = 0.03$, $q_2(0) = 0.01$, $\dot{q}_2(0) = 0$ in each presented time simulation. The initial conditions for the nonlinear attachment are $y(0) = 0.01$, $\dot{y}(0) = 0$ and $Q(0) = 0$. Time responses are obtained for the coordinates $q_1(\tau)$, $q_2(\tau)$, $y(\tau)$ and $\dot{Q}(\tau)$, by using the direct numerical integration (ode45 in Matlab) and solving the system equations Eq.(22) - Eq.(25) for time period $T = 150$. Figures 12 - 15 show time response diagrams for different values of transporting sped $v = 0.2, 0.4, 0.6$ and 0.8. It should be noted the blue solid lines represent the amplitude of the primary structure without a nonlinear attachment, the red solid lines show the amplitudes of the primary structure, and the green solid lines are related to the amplitude of the NES mass (for Fig.12 - Fig.15, sub-figures (a) and (b)). In all cases, sub-figures (c) shows the electric current responses during a long time integration.

One can observe that the introduced NES-EH device has a large effect on the response amplitudes, which is displayed in the form of reduced amplitude of the primary structure. The main reason for this lies in the transfer of mechanical energy from the excited axially moving beam structure to the NES-EH attachment, which is then dissipated through the mechanical NES damping. Part of that energy can be captured by the introduced EH device, as shown in sub-figures (c) (Fig.12 - Fig.15). By comparing the response amplitudes

Journal Pre-proof

Journal Pre-proof

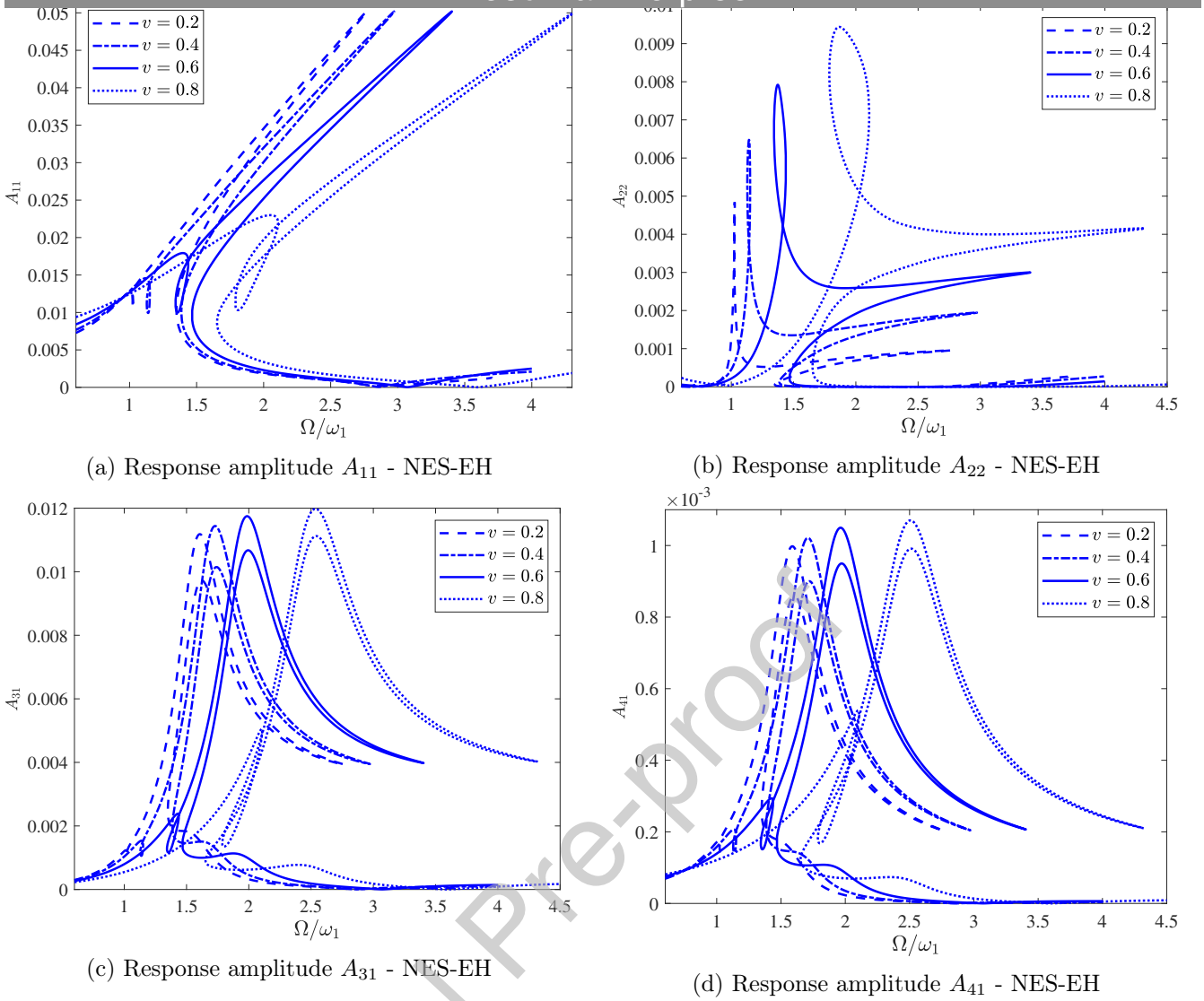

(a) Response amplitude A_{11} - NES-EH

(b) Response amplitude A_{22} - NES-EH

(c) Response amplitude A_{31} - NES-EH

(d) Response amplitude A_{41} - NES-EH

Figure 11: The amplitude-frequency response curves A_{11}, A_{22} and A_{31} and A_{41} of the axially moving beam with nonlinear NES-EH attachments for different values of transporting speed v, and linear stiffness parameter $\tilde{k}_p$ and excitation load $f_1 = 0.07$.

$q_1(\tau)$ and $q_2(\tau)$ from Fig.12 - Fig.15, it can be observed that amplitudes of $q_1(\tau)$ and $q_2(\tau)$ of the system with NES-EH device decrease much faster then those for the case with the primary structure alone. After investigating the effects of the transporting speed v on vibration attenuation, it can be concluded that an increase of this parameter leads to minor changes in the amplitudes $q_1(\tau)$ and $q_2(\tau)$ at the beginning of the simulation. At the same time, the energy harvesting application can be analyzed through the series of A_{41} response amplitude diagrams given in sub-figures (c) (Fig.12 - Fig.15). It can be observed that for lower values of transporting speed v responses $\dot{Q}$ are higher at the beginning of the simulation and then rapidly decrease due to imposed vibration reduction through NES-EH device. On the other hand, higher values of transporting speed v lead to higher initial response amplitudes, which after reaching the peak value gradually decrease to some finitely small value. Based on such behavior, it can be pointed out that the presented nonlinear attachment, such as a NES-EH device, shows great performance in energy localization and dissipation characteristics in short time intervals.

In this study, we paid more attention to the performance of NES-EH device than those of pure NES since there is no significant difference in their behavior when comparing their effects on the reduction of vibration amplitudes. In this study both NES and NES-EH configurations were investigated, but the attention was focused primarily on NES-EH since the results indicated that there was no significant difference in their performance regarding the vibration attenuation. So it can be concluded that introducing the EH element does not by itself improve the vibration reduction capabilities of the device. Nevertheless, compared to the regular NES, a NES-EH has another important additional property - it can transform some of the mechanical vibration energy into electrical energy, that is, such a device possesses energy harvesting capabilities. However, the presented analysis also showed certain drawbacks of the proposed NES-EH device configuration

Journal Pre-proof

Journal Pre-proof

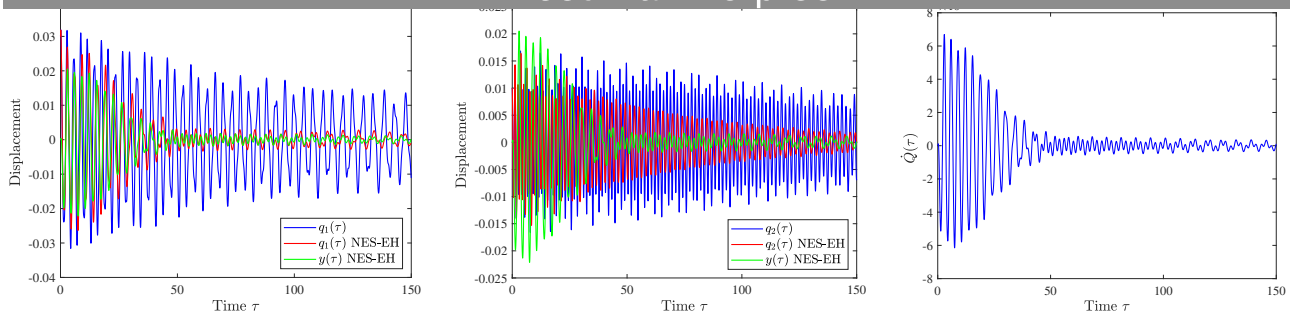

Figure 12: The time response diagrams for the transporting speed $v = 0.2$.

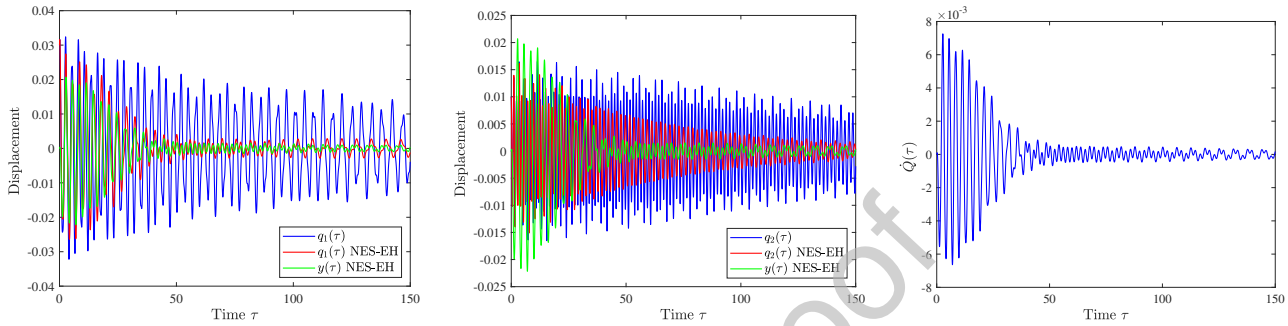

Figure 13: The time response diagrams for the transporting speed $v = 0.4$.

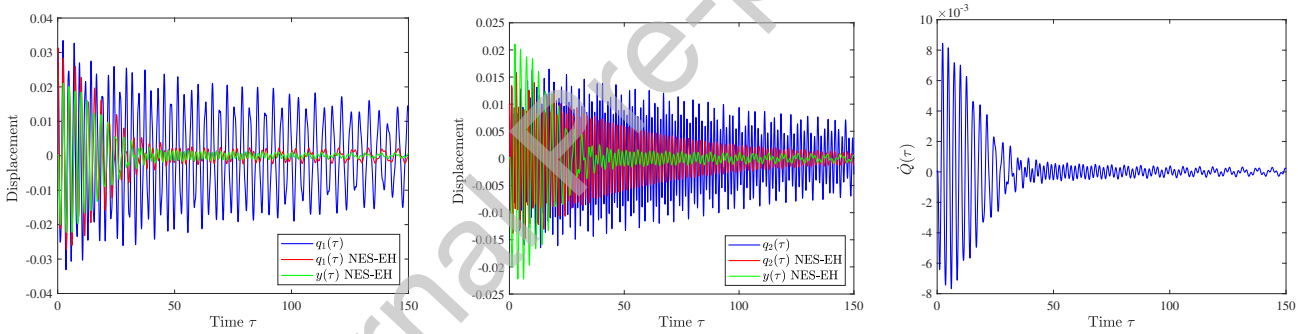

Figure 14: The time response diagrams for the transporting speed $v = 0.6$.

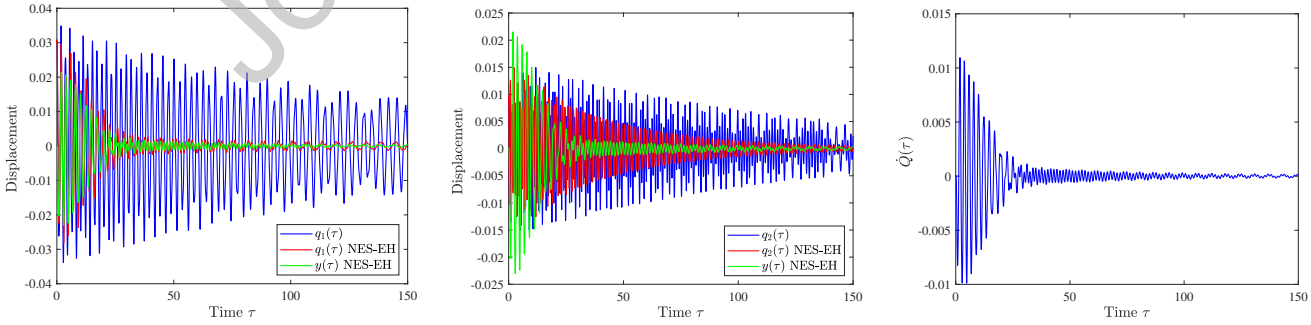

Figure 15: The time response diagrams for the transporting speed $v = 0.8$.

i.e. it demonstrated that the portion of the harvested energy is relatively small and that it depends on how fast the NES will transfer the energy from the main structure to the attachment and dissipate it through the mechanical damper. In spite of that, the amount of harvested electrical energy could be sufficient to supply some small monitoring devices and sensors such as MEMS or NEMS.

Journal Pre-proof

Journal Pre-proof

7. Conclusions

In this paper we used a semi-numerical approach to study the nonlinear periodic responses of an axially moving beam with nonlinear attachment such as a nonlinear energy sink coupled with an energy harvesting device. We have shown that by attaching this device onto the primary structure one can exploit both vibration suppression and energy harvesting capabilities of the presented system. The governing equations of the system are derived by using the Euler-Bernoulli beam theory, von KÃąrmÃąn strain-displacement relation and Hamilton's principle. The Galerkin method is introduced to discretize the partial differential equations to the system of nonlinear ordinary differential equations. Two sources of nonlinearity are considered - the geometric nonlinearity that introduces the large amplitude deflections into the system, as well as a nonlinearity of the spring in the nonlinear energy sink device. The problem of finding the periodic responses in the form of amplitude-frequency diagrams is resolved by using the semi-numerical IHB and continuation method. This methodology significantly simplifies the calculation of periodic solutions compared to the classical numerical integration methods, thus very efficiently providing the complex amplitude-frequency responses of strongly nonlinear systems with turning points and multiple periodic solutions. Complete set of integrals for IHB is derived in the analytic form, where the computation time for determination of responses is significantly reduced. Application of the Floquet stability theory and the Hsu procedure to investigate the stability of a periodic solution significantly improved the qualitative analysis of the system's nonlinear behavior. Considering the direct numerical integration, the time response diagrams are determined to study the amplitude response reduction and energy localization and dissipation through the application of the NES-EH attachment. Validation study have shown a good agreement of the results obtained by the presented method with the results from the literature. Parametric study revealed that performance of the nonlinear attachment becomes more prominent for an increase of the linear stiffness and transporting speed. Moreover, it was shown that an increase of the transporting speed leads to amplification of the hardening stiffness nonlinearity effect.

Since undesired vibration of engineering structures can be induced by various sources such as earthquakes, acoustic noise, machine or vehicle-induced vibration or flow-induced vibration, introduction of the NES or coupled NES-EH devices can be advantageous for vibration absorption and energy harvesting purposes. Based on the presented results, it can be concluded that methodology used in this study can be applied to analyze systems with higher number of structural elements and degrees of freedom with strong nonlinearities, which can be an important step in future design of novel passive vibration control devices.

Journal Pre-proof

Acknowledgments

D. Karličić was supported by the Marie SkÅĆodowska-Curie Actions - European Commission: 799201-METACTIVE. M. Cajić and S. Paunović were sponsored by the Serbian Ministry of Education, Science and Technological Development and Mathematical Institute SANU.

References

[1] Wang Lin and Ni Qiao. Vibration and stability of an axially moving beam immersed in fluid. *International journal of solids and structures*, 45(5):1445–1457, 2008.

[2] Kefei Zhu and Jintai Chung. Vibration and stability analysis of a simply-supported rayleigh beam with spinning and axial motions. *Applied Mathematical Modelling*, 66:362–382, 2019.

[3] Phuong-Tung Pham and Keum-Shik Hong. Dynamic models of axially moving systems: A review. *Nonlinear Dynamics*, 100:315–349, 2020.

[4] Zheng Lu, Zixin Wang, Ying Zhou, and Xilin Lu. Nonlinear dissipative devices in structural vibration control: A review. *Journal of Sound and Vibration*, 423:18–49, 2018.

[5] Hu Ding Li-Qun Chen. Designs, analysis, and applications of nonlinear energy sinks. *Nonlinear Dynamics*, 100:3061–3107, 2020.

[6] Alexander F Vakakis. Inducing passive nonlinear energy sinks in vibrating systems. *Journal of Vibration and Acoustics*, 123(3):324–332, 2001.

[7] Alexander F Vakakis, Oleg V Gendelman, Lawrence A Bergman, D Michael McFarland, Gaëtan Kerschen, and Young Sup Lee. *Nonlinear targeted energy transfer in mechanical and structural systems*, volume 156. Springer Science & Business Media, 2008.

[8] Fotios Georgiades and Alexander F Vakakis. Dynamics of a linear beam with an attached local nonlinear energy sink. *Communications in Nonlinear Science and Numerical Simulation*, 12(5):643–651, 2007.

[9] Oleg V Gendelman. Bifurcations of nonlinear normal modes of linear oscillator with strongly nonlinear damped attachment. *Nonlinear Dynamics*, 37(2):115–128, 2004.

Journal Pre-proof

[10] Claude-Henri Lamarque, Oleg V Gendelman, Alireza Ture Savadkoohi, and Emilie Etcheverria. Targeted energy transfer in mechanical systems by means of non-smooth nonlinear energy sink. *Acta mechanica*, 221(1-2):175, 2011.

[11] Y Starosvetsky and OV Gendelman. Vibration absorption in systems with a nonlinear energy sink: nonlinear damping. *Journal of Sound and Vibration*, 324(3-5):916–939, 2009.

[12] OV Gendelman and A Alloni. Dynamics of forced system with vibro-impact energy sink. *Journal of Sound and Vibration*, 358:301–314, 2015.

[13] Etienne Gourc, Sebastien Seguy, Guilhem Michon, Alain Berlioz, and BP Mann. Quenching chatter instability in turning process with a vibro-impact nonlinear energy sink. *Journal of Sound and Vibration*, 355:392–406, 2015.

[14] Xianren Kong, Haiqin Li, and Chen Wu. Dynamics of 1-dof and 2-dof energy sink with geometrically nonlinear damping: application to vibration suppression. *Nonlinear Dynamics*, 91(1):733–754, 2018.

[15] Javad Taghipour and Morteza Dardel. Steady state dynamics and robustness of a harmonically excited essentially nonlinear oscillator coupled with a two-dof nonlinear energy sink. *Mechanical Systems and Signal Processing*, 62:164–182, 2015.

[16] Z Nili Ahmadabadi and SE Khadem. Nonlinear vibration control and energy harvesting of a beam using a nonlinear energy sink and a piezoelectric device. *Journal of Sound and Vibration*, 333(19):4444–4457, 2014.

[17] Xiaoai Jiang, D Michael McFarland, Lawrence A Bergman, and Alexander F Vakakis. Steady state passive nonlinear energy pumping in coupled oscillators: theoretical and experimental results. *Nonlinear Dynamics*, 33(1):87–102, 2003.

[18] Emmanuel Gourdon, Nicholas A Alexander, Colin A Taylor, Claude-Henri Lamarque, and Stéphane Pernot. Nonlinear energy pumping under transient forcing with strongly nonlinear coupling: Theoretical and experimental results. *Journal of sound and vibration*, 300(3-5):522–551, 2007.

[19] Rajab A Malookani and Wim T van Horssen. On the asymptotic approximation of the solution of an equation for a non-constant axially moving string. *Journal of Sound and Vibration*, 367:203–218, 2016.

[20] Daniel Hochlenert, Gottfried Spelsberg-Korspeter, and Peter Hagedorn. Friction induced vibrations in moving continua and their application to brake squeal. *Journal of Applied Mechanics*, 74(3):542–549, 2007.

[21] Tianzhi Yang, Tao Liu, Ye Tang, Shuai Hou, and Xiaofei Lv. Enhanced targeted energy transfer for adaptive vibration suppression of pipes conveying fluid. *Nonlinear Dynamics*, pages 1–8, 2018.

[22] Ye-Wei Zhang, Hao Zhang, Shuai Hou, Ke-Fan Xu, and Li-Qun Chen. Vibration suppression of composite laminated plate with nonlinear energy sink. *Acta Astronautica*, 123:109–115, 2016.

[23] Youssef Bichiou, Muhammad R Hajj, and Ali H Nayfeh. Effectiveness of a nonlinear energy sink in the control of an aeroelastic system. *Nonlinear Dynamics*, 86(4):2161–2177, 2016.

[24] Gottfried Spelsberg-Korspeter, Oleg N Kirillov, and Peter Hagedorn. Modeling and stability analysis of an axially moving beam with frictional contact. *Journal of Applied Mechanics*, 75(3):031001, 2008.

[25] Ye-Wei Zhang, Yan-Nan Lu, Wei Zhang, Ying-Yuan Teng, Hui-Xin Yang, Tian-Zhi Yang, and Li-Qun Chen. Nonlinear energy sink with inerter. *Mechanical Systems and Signal Processing*, 125:52–64, 2019.

[26] Zhen Zhang, Ze-Qi Lu, Hu Ding, and Li-Qun Chen. An inertial nonlinear energy sink. *Journal of Sound and Vibration*, 450:199–213, 2019.

[27] Ye-Wei Zhang, Zhen Zhang, Li-Qun Chen, Tian-Zhi Yang, Bo Fang, and Jian Zang. Impulse-induced vibration suppression of an axially moving beam with parallel nonlinear energy sinks. *Nonlinear dynamics*, 82(1-2):61–71, 2015.

[28] Ye-Wei Zhang, Bin Yuan, Bo Fang, and Li-Qun Chen. Reducing thermal shock-induced vibration of an axially moving beam via a nonlinear energy sink. *Nonlinear Dynamics*, 87(2):1159–1167, 2017.

[29] Kai Yang, Ye-Wei Zhang, Hu Ding, Tian-Zhi Yang, Yang Li, and Li-Qun Chen. Nonlinear energy sink for whole-spacecraft vibration reduction. *Journal of Vibration and Acoustics*, 139(2):021011, 2017.

[30] Ye-Wei Zhang, Jian Zang, Tian-Zhi Yang, Bo Fang, and Xin Wen. Vibration suppression of an axially moving string with transverse wind loadings by a nonlinear energy sink. *Mathematical Problems in Engineering*, 2013, 2013.

[31] Daniele Zulli and Angelo Luongo. Nonlinear energy sink to control vibrations of an internally nonresonant elastic string. *Meccanica*, 50(3):781–794, 2015.

[32] Angelo Luongo and Daniele Zulli. Nonlinear energy sink to control elastic strings: the internal resonance case. *Nonlinear Dynamics*, 81(1-2):425–435, 2015.

[33] Max-Uwe Noll, Lukas Lentz, and Utz von Wagner. On the discretization of a bistable cantilever beam with application to energy harvesting. *Facta Universitatis, Series: Mechanical Engineering*, 17(2):125–139, 2019.

[34] Daniel Kremer and Kefu Liu. A nonlinear energy sink with an energy harvester: transient responses. *Journal of sound and vibration*, 333(20):4859–4880, 2014.

[35] Daniel Kremer and Kefu Liu. A nonlinear energy sink with an energy harvester: Harmonically forced responses. *Journal of Sound and Vibration*, 410:287–302, 2017.

[36] Yu Zhang, Lihua Tang, and Kefu Liu. Piezoelectric energy harvesting with a nonlinear energy sink. *Journal of Intelligent Material Systems and Structures*, 28(3):307–322, 2017.

[37] Xiang Li, Ye-Wei Zhang, Hu Ding, and Li-Qun Chen. Dynamics and evaluation of a nonlinear energy sink integrated by a piezoelectric energy harvester under a harmonic excitation. *Journal of Vibration and Control*, 25(4):851–867, 2019.

[38] Antoine Blanchard, Lawrence A Bergman, and Alexander F Vakakis. Vortex-induced vibration of a linearly sprung cylinder with an internal rotational nonlinear energy sink in turbulent flow. *Nonlinear Dynamics*, pages 1–17, 2019.

[39] PV Rasil Raj and B Santhosh. Parametric study and optimization of linear and nonlinear vibration absorbers combined with piezoelectric energy harvester. *International Journal of Mechanical Sciences*, 152:268–279, 2019.

[40] Kevin Remick, D Dane Quinn, D Michael McFarland, Lawrence Bergman, and Alexander Vakakis. High-frequency vibration energy harvesting from impulsive excitation utilizing intentional dynamic instability caused by strong nonlinearity. *Journal of Sound and Vibration*, 370:259–279, 2016.

[41] MJ Leamy and NC Perkins. Nonlinear periodic response of engine accessory drives with dry friction tensioners. 1998.

[42] Peter Hagedorn and Anirvan DasGupta. *Vibrations and waves in continuous mechanical systems*. Wiley Online Library, 2007.

[43] JA Wickert. Non-linear vibration of a traveling tensioned beam. *International Journal of Non-Linear Mechanics*, 27(3):503–517, 1992.

Journal Pre-proof

Journal Pre-proof

[44] JL Huang, RKL Su, WH Li, and SH Chen. Stability and bifurcation of an axially moving beam tuned to three-to-one internal resonances. *Journal of Sound and Vibration*, 330(3):471–485, 2011.
[45] KY Sze, SH Chen, , and JL Huang. The incremental harmonic balance method for nonlinear vibration of axially moving beams. *Journal of sound and vibration*, 281(3-5):611–626, 2005.
[46] M Ouled Chtiba, S Choura, AH Nayfeh, and S El-Borgi. Vibration confinement and energy harvesting in flexible structures using collocated absorbers and piezoelectric devices. *Journal of Sound and Vibration*, 329(3):261–276, 2010.
[47] Francesco Pellicano and F Vestroni. Nonlinear dynamics and bifurcations of an axially moving beam. *Journal of Vibration and Acoustics*, 122(1):21–30, 2000.
[48] Shihua Zhou, Guiqiu Song, Zhaohui Ren, and Bangchun Wen. Nonlinear analysis of a parametrically excited beam with intermediate support by using multi-dimensional incremental harmonic balance method. *Chaos, Solitons & Fractals*, 93:207–222, 2016.
[49] Xuefeng Wang, Weidong Zhu, and Xi Zhao. An incremental harmonic balance method with a general formula of jacobian matrix and a direct construction method in stability analysis of periodic responses of general nonlinear delay differential equations. *Journal of Applied Mechanics*, 86(6):061011, 2019.
[50] Udbhau Bhattiprolu, Anil K Bajaj, and Patricia Davies. Periodic response predictions of beams on nonlinear and viscoelastic unilateral foundations using incremental harmonic balance method. *International Journal of Solids and Structures*, 99:28–39, 2016.
[51] AYT Leung and SK Chui. Non-linear vibration of coupled duffing oscillators by an improved incremental harmonic balance method. *Journal of Sound and Vibration*, 181(4):619–633, 1995.
[52] Rüdiger Seydel. *Practical bifurcation and stability analysis*, volume 5. Springer Science & Business Media, 2009.
[53] Chieh Su Hsu. Impulsive parametric excitation: theory. *International Journal of Mechanical Sciences*, 39(2):551–558, 1972.
[54] P Friedmann, CE Hammond, and Tze-Hsin Woo. Efficient numerical treatment of periodic systems with application to stability problems. *International Journal for Numerical Methods in Engineering*, 11(7):1117–1136, 1977.
[55] Ali H Nayfeh and Balakumar Balachandran. *Applied nonlinear dynamics: analytical, computational, and experimental methods*. John Wiley & Sons, 2008.
[56] CH Riedel and CA Tan. Coupled, forced response of an axially moving strip with internal resonance. *International Journal of Non-Linear Mechanics*, 37(1):101–116, 2002.
[57] JL Huang, RKL Su, and SH Chen. Precise hsuâĂŹs method for analyzing the stability of periodic solutions of multi-degrees-of-freedom systems with cubic nonlinearity. *Computers & structures*, 87(23-24):1624–1630, 2009.

Appendix 1: Matrix coefficients

Matrices and vectors in Eq.(22):

$$\mathbf{K}_{11}=\int_0^{2\pi}\left\{\Omega_0^2\mathbf{C}^T\mathbf{C}''+\Omega_0(\mu_{11}+2b)\mathbf{C}^T\mathbf{C}'+\left(k_{11}+k_{12}q_{20}^2+3k_{13}q_{10}^2+6kq_{10}^2-12kq_{10}y_0+6ky_0^2\right)\mathbf{C}^T\mathbf{C}\right\}d\tau, \tag{46}$$

$$\mathbf{K}_{12}=\int_0^{2\pi}\left\{\mu_{12}\Omega_0\mathbf{C}^T\mathbf{C}'+2k_{12}q_{10}q_{20}\mathbf{C}^T\mathbf{C}\right\}d\tau,$$

$$\mathbf{K}_{13}=\int_0^{2\pi}\left\{-2b\Omega_0\mathbf{C}^T\mathbf{C}'+6k(-q_{10}^2+2q_{10}y_0-y_0^2)\mathbf{C}^T\mathbf{C}\right\}d\tau,$$

$$\mathbf{R}_{11}=-\int_0^{2\pi}\left\{\Omega_0^2\mathbf{C}^T\mathbf{C}''+\Omega_0(\mu_{11}+2b)\mathbf{C}^T\mathbf{C}'+\left(k_{11}+k_{13}q_{10}^2+2kq_{10}^2\right)\mathbf{C}^T\mathbf{C}\right\}d\tau,$$

$$\mathbf{R}_{12}=-\int_0^{2\pi}\left\{-\Omega_0\mu_{12}\mathbf{C}^T\mathbf{C}'+k_{12}q_{10}q_{20}\mathbf{C}^T\mathbf{C}\right\}d\tau,$$

$$\mathbf{R}_{13}=-\int_0^{2\pi}\left\{-2b\Omega_0\mathbf{C}^T\mathbf{C}'+2k\left(-3q_{10}^2+3q_{10}y_0-y_0^2\right)\mathbf{C}^T\mathbf{C}\right\}d\tau,$$

$$\mathbf{V}_{11}=-\int_0^{2\pi}\left\{2\Omega_0\mathbf{C}^T\mathbf{C}''+(\mu_{11}+2b)\mathbf{C}^T\mathbf{C}'\right\}d\tau,$$

$$\mathbf{V}_{12}=-\int_0^{2\pi}\left\{-\mu_{12}\mathbf{C}^T\mathbf{C}'\right\}d\tau,$$

$$\mathbf{V}_{13}=-\int_0^{2\pi}\left\{-2b\mathbf{C}^T\mathbf{C}'\right\}d\tau,$$

$$\tilde{\mathbf{F}}_1=\int_0^{2\pi}\left\{f_1\mathbf{C}^T\cos\tau\right\}d\tau,$$

Matrices and vectors in Eq.(23):

$$\mathbf{K}_{21} = \int_0^{2\pi} \left\{ \mu_{21}\Omega_0 \mathbf{C}^T\mathbf{C}' + 2k_{22}q_{10}q_{20}\mathbf{C}^T\mathbf{C} \right\} d\tau, \tag{47}$$

$$\mathbf{K}_{22} = \int_0^{2\pi} \left\{ \Omega_0^2 \mathbf{C}^T\mathbf{C}'' + \Omega_0\mu_{22}\mathbf{C}^T\mathbf{C}' + \left(k_{21} + k_{22}q_{10}^2 + 3k_{23}q_{20}^2\right)\mathbf{C}^T\mathbf{C} \right\} d\tau,$$

$$\mathbf{R}_{21} = -\int_0^{2\pi} \left\{ -\Omega_0\mu_{21}\mathbf{C}^T\mathbf{C}' + k_{22}q_{10}q_{20}\mathbf{C}^T\mathbf{C} \right\} d\tau,$$

$$\mathbf{R}_{22} = -\int_0^{2\pi} \left\{ \Omega_0^2 \mathbf{C}^T\mathbf{C}'' + \Omega_0\mu_{22}\mathbf{C}^T\mathbf{C}' + \left(k_{21} + k_{23}q_{20}^2\right)\mathbf{C}^T\mathbf{C} \right\} d\tau,$$

$$\mathbf{V}_{21} = -\int_0^{2\pi} \left\{ \mu_{21}\mathbf{C}^T\mathbf{C}' \right\} d\tau,$$

$$\mathbf{V}_{22} = -\int_0^{2\pi} \left\{ 2\Omega_0\mathbf{C}^T\mathbf{C}'' + \mu_{22}\mathbf{C}^T\mathbf{C}' \right\} d\tau,$$

$$\tilde{\mathbf{F}}_2 = \int_0^{2\pi} \left\{ f_2\mathbf{C}^T\cos\tau \right\} d\tau,$$

Matrices from Eq.(24):

$$\mathbf{K}_{31} = \int_0^{2\pi} \left\{ -b\Omega_0\mathbf{C}^T\mathbf{C}' - k(3q_{10}^2 - 6q_{10}y_0 + 3y_0^2)\mathbf{C}^T\mathbf{C} \right\} d\tau, \tag{48}$$

$$\mathbf{K}_{33} = \int_0^{2\pi} \left\{ \varepsilon\Omega_0^2 \mathbf{C}^T\mathbf{C}'' + \Omega_0 b\mathbf{C}^T\mathbf{C}' + \tilde{k}_p\mathbf{C}^T\mathbf{C} - k\left(-3q_{10}^2 + 6q_{10}y_0 - 3y_0^2\right)\mathbf{C}^T\mathbf{C} \right\} d\tau,$$

$$\mathbf{K}_{34} = \int_0^{2\pi} \left\{ -\tilde{G}\mathbf{C}^T\mathbf{C} \right\} d\tau,$$

$$\mathbf{R}_{31} = -\int_0^{2\pi} \left\{ -b\Omega_0\mathbf{C}^T\mathbf{C}' - k\left(q_{10}^2 - 3q_{10}y_0\right)\mathbf{C}^T\mathbf{C} \right\} d\tau,$$

$$\mathbf{R}_{33} = -\int_0^{2\pi} \left\{ \Omega_0^2\varepsilon\mathbf{C}^T\mathbf{C}'' + \tilde{k}_p\mathbf{C}^T\mathbf{C} + \Omega_0 b\mathbf{C}^T\mathbf{C}' + k\left(y_0^2 - 3q_{10}y_0\right)\mathbf{C}^T\mathbf{C} \right\} d\tau,$$

$$\mathbf{R}_{34} = -\int_0^{2\pi} \left\{ -\tilde{G}\mathbf{C}^T\mathbf{C} \right\} d\tau,$$

$$\mathbf{V}_{31} = -\int_0^{2\pi} \left\{ -b\mathbf{C}^T\mathbf{C}' \right\} d\tau,$$

$$\mathbf{V}_{33} = -\int_0^{2\pi} \left\{ 2\Omega_0\varepsilon\mathbf{C}^T\mathbf{C}'' + b\mathbf{C}^T\mathbf{C}' \right\} d\tau,$$

Matrices from Eq.(25):

$$\mathbf{K}_{43} = -\int_0^{2\pi} \left\{ \mathbf{C}^T\mathbf{C} \right\} d\tau,$$

$$\mathbf{K}_{44} = \int_0^{2\pi} \left\{ \tilde{R}\Omega_0\mathbf{C}^T\mathbf{C}' + \mathbf{C}^T\mathbf{C} \right\} d\tau,$$

$$\mathbf{R}_{43} = -\int_0^{2\pi} \left\{ -\mathbf{C}^T\mathbf{C} \right\} d\tau,$$

$$\mathbf{R}_{44} = -\int_0^{2\pi} \left\{ \tilde{R}\Omega_0\mathbf{C}^T\mathbf{C}' + \mathbf{C}^T\mathbf{C} \right\} d\tau,$$

$$\mathbf{V}_{44} = -\int_0^{2\pi} \left\{ \tilde{R}\Omega_0\mathbf{C}^T\mathbf{C}' \right\} d\tau.$$

Journal Pre-proof

Journal Pre-proof

Author Statement

Danilo Karlicic: Software, Writing- Original draft preparation. Milan Cajic: Conceptualization, Validation. Stepa Paunovic: Software, Writing âĂŞ review & editing. Sonipon Adhikari: Editing and Supervision.

Declaration of interests

The authors declare that they have no known competing financial interests or personal relationships that could have appeared to influence the work reported in this paper.

Journal Pre-proof